International Journal of Solids and Structures 49 (2012) 1434–1452

Contents lists available at SciVerse ScienceDirect

International Journal of Solids and Structures

journal homepage: www.elsevier.com/locate/ijsolstr

The fracture behaviour of adhesively-bonded composite joints: Effects of rate of test and mode of loading

B.R.K. Blackman *, A.J. Kinloch, F.S. Rodriguez-Sanchez, W.S. Teo

Department of Mechanical Engineering, Imperial College London, South Kensington Campus, London SW7 2AZ, UK

ARTICLE INFO

Article history:
Received 25 August 2011
Received in revised form 25 January 2012
Available online 6 March 2012

Keywords:
Adhesive joints
Composites
Dynamic effects
Fracture mechanics
High rate
Mode of loading

ABSTRACT

The present paper discusses the results of an investigation into the effects of test rate and the mode of loading on the fracture energy, G_c, of adhesively-bonded fibre-composite joints. Various carbon-fibre reinforced-polymer (CFRP) matrix composite substrates have been bonded using two different types of automotive structural epoxy-adhesives. They have been tested via loading the bonded joints in mode I (tensile), mode II (in-plane shear) and mixed-mode I/II from slow rates (i.e., of about 10^{-5} m/s) up to relatively high rates of test of about 15 m/s. The high-rate tests were photographed using a high-speed digital video camera to record the deformation of the joint and the fracture behaviour. An analysis strategy has been developed for the various modes of loading (i) to account for the observed fracture behaviour, (ii) to circumvent the problems posed by oscillations in the load traces due to the presence of dynamic effects in the faster tests, and (iii) to account for the kinetic energy associated with the moving specimen arms in the faster tests. Based on the analysis strategy developed, the effect of the test rate on the fracture energy, G_c, for the different loading modes for the joints has been ascertained. Furthermore, various different fracture paths were observed in the tests. They were either cohesive, in the adhesive layer, or interlaminar in the composite substrates. The exact fracture path observed was a function of (i) the type of composite substrate, (ii) the type of adhesive, and (iii) the mode of loading employed. However, the nature of the fracture path was found to be quite insensitive to the test rate. Essentially, it was found that joints subjected to mixed-mode I/II loading were more likely to exhibit an interlaminar fracture path in the composite substrates than when loaded in either pure modes I or II. The propensity for a given joint to exhibit such a fracture path via delamination of the composite substrate has been explained by calculating the transverse tensile stresses induced in the loaded composite arms, and comparing this value to the measured transverse tensile strength of the composite. Following this approach, the underlying reasons for the observed fracture path were identified and could be predicted. Also, the proposed scheme provides a route to design against delamination failure occurring in adhesively-bonded fibre-composite test specimens.

1. Introduction

The drive to reduce vehicle weight in the automotive industry has led to the increased use of composite materials and lightweight alloys in the construction of modern cars (Wall et al., 2004). Indeed, the effort to produce lightweight vehicle structures has prompted designers to implement multi-materials solutions in their latest models. However, the use of many very different materials within a single vehicle structure poses many challenges, an important one being the need to join successfully the different materials. A further challenge is to ensure that the resulting structures comply with the ever-increasing safety standards. Adhesive bonding is a key enabling technology in the pursuit of lightweight, energy absorbing vehicle structures, and adhesives represent a very efficient means of joining dissimilar materials. Indeed, the use of structural epoxy adhesives have been shown to lead to the manufacture of vehicle structures that deform in a progressive, and highly energy-absorbing, manner when subjected to collision. This is achieved by ensuring that premature brittle failure within the joint is avoided, and then enabling large-scale plastic deformation of metallic parts, or crumpling with associated multiple damage mechanisms in composite parts, to occur. This need to avoid premature brittle failure of the adhesive obviously emphasises the importance of assessing the toughness of adhesively-bonded joints when subjected to relatively high rates of test and different modes of loading.

Various workers have investigated the combined effects of test rate and mode mix on the fracture performance of adhesively bonded joints. Simon et al. (2005) developed a modified drop tower to determine the fracture resistance of adhesively bonded automotive composite joints to modes I, II and mixed-mode I/II loading.

* Corresponding author. Tel.: +44 2075947196; fax: +44 2075947011.
E-mail address: b.blackman@imperial.ac.uk (B.R.K. Blackman).

0020-7683/$ - see front matter © 2012 Elsevier Ltd. All rights reserved.
doi:10.1016/j.ijsolstr.2012.02.022

Nomenclature

a	crack length measured from load-line or left hand support
a_c	effective crack length calculated from compliance in a mode II test
B	width of test specimen
C	compliance of the joint, given by δ/P
c_L	longitudinal wave speed in the substrate material
E_1	Young's modulus of the substrate, in the longitudinal direction
F	Large displacement correction factor for specified test geometry
G^s	the energy release rate for a symmetrically-loaded DCB
G_{Ic}	the adhesive fracture energy in mode I
G^s_{Ic}	the static value of the adhesive fracture energy
G^d_{Ic}	the dynamically-corrected value of G_{Ic}
G_{IIc}	the adhesive fracture energy in mode II
G^d_{IIc}	the dynamically corrected value of G_{IIc}
$G_{I/IIc}$	the adhesive fracture energy in mixed-mode
$G^d_{I/IIc}$	the dynamically corrected value of $G_{I/IIc}$
h	height of the beam, i.e., arm of the substrate
k	mixed-mode linear interaction parameter
L	free length of the specimen in the ELS test or the half span length in the ENF and MMF tests
N	load-block stiffening correction factor for specified test geometry
P	load applied to the test specimen
t	test time from the onset of loading
t_i	test time from the onset of loading to that required for the initiation of crack growth
t_o	time at the initial position of the joint before loading
V	velocity of the load-point, as measured using high-speed video photography
α	transverse stress coefficients in modes I, II or mixed-mode I/II
χ	correction factor for beam root rotation and transverse shear
δ	load-line displacement of the specimen during a test
Δ_I	mode I beam root rotation correction
Δ_{II}	mode II beam root rotation correction
ν	Poisson's ratio of the substrate material
ρ_s	density of the substrate material
σ_{yyc}	transverse tensile strength of the substrate
σ_{yy}	transverse tensile stress on the substrate

Loading rates of up to 3.7 m/s were obtained and a high speed video camera running at up to 2000 fps was used to record the tests. The occurrence of unsteady crack growth complicated the interpretation of the results. Sun et al. (2008a,b, 2009a,b) studied the effects of test rate and loading mode on plastically deforming joints using a commercial adhesive to join dual-phase steel substrates. In mode I (Sun et al., 2008a,b) a fully cohesive, quasi-static mode of failure associated with high toughness was observed at slower rates and a more brittle mode of failure associated with lower toughness was observed at the faster rates. The transition from the ductile to the brittle regime led to reductions in toughness by up to a factor of five. The quasi-static fracture resistance was found to be quite insensitive to test rate, and the main rate effect was identified as being the increased probability of triggering the transition. In mode II loading (Sun et al., 2009a), failure occurred along (or close to) the adhesive-steel interface but no transitions were observed from the quasi-static to dynamic failure mode however, the authors noted differences in plastic hinge behaviour in the substrates. Values of G_{IIc} were found to increase somewhat with increasing test rate, although the increase was within the range of scatter in the results. In mixed-mode loading using an asymmetric DCB specimen, failure again occurred along the adhesive-steel interface (along the interface with the thinner substrate) and the authors commented that transitions from the ductile to the brittle mode of failure appeared to be stochastic in nature, with an intermediate rate showing a transition, but a faster and slower rate not doing so. Thus the combined effects of test rate and mode mixity were described in terms of (i) fracture path selection (ii) the cohesive parameters relevant for each mode and (iii) the apparently random occurrence of transitions between ductile and brittle fracture behaviour. Dillard et al. (2009) discussed the effects of loading mode on fracture path selection in more complex, multilayered materials. They noted that failure paths, and indeed fracture behaviour, is frequently much more complicated in such materials and that the fracture path can dominate the measured toughness when these materials are adhesively bonded. The authors commented that failure criteria which have been developed to model the observed mixed-mode fracture resistance are phenomenological in nature and are thus inappropriate when changes to the failure path occur.

The aims of the present research have been to develop, using a fracture mechanics approach, a test methodology and associated analysis strategy to evaluate the performance of adhesively-bonded fibre-composite joints in terms of the fracture energy, G_c, as a function of the test rate and the mode of loading. A linear-elastic fracture-mechanics (LEFM) approach has been employed and the detailed procedures developed for mode I (tensile opening) fracture were published in recent papers (Blackman et al., 2009; Karac et al., 2011). Thus, whilst additional mode I results are presented here, the present work additionally focuses on the effects of mode II (in-plane shear) and mixed-mode (I/II) loading. The present paper first gives the details of the adhesives and composite substrates which have been employed and then outlines the types of test which have been undertaken, both at quasi-static and at relatively high rates of test. The following two sections of the paper then discuss the methods of analysis and the results from the mode I, mode II and mixed-mode I/II tests under quasi-static and the high-test of test, respectively. One very interesting aspect which arises from these results is the apparently complex, and different, failure paths which are observed in the various types of joints, under the various rates of test. Thus, we have proposed a model to describe the different failure loci observed and the results from this model are compared to the experimental results in the penultimate section of the paper. In the final section of the paper the different themes are brought together to give our overall conclusions.

2. Experimental

2.1. Materials

In this investigation, joints were prepared with one of two structural epoxy adhesives, as given in Table 1. The first adhesive, 'Betamate XD4600', is commonly used in automotive bonding and was supplied as a single-part epoxy-paste by Dow Automotive (Switzerland). The second adhesive, 'SIA PL731', was supplied by Sovereign Speciality Adhesives Inc. (USA). This adhesive is a two-part epoxy system supplied in cartridges with a resin-to-hardener ratio of 4:1. The resin and hardener were mixed in a centrifugal mixer for 1.5 min at 3000 rpm to ensure proper mixing. This adhe-

Table 1
Details of the adhesives used.

Adhesive	Designation	Form (colour)	Cure temp (°C)	Cure time (min)	T_g (°C)
XD4600	XD4600	One part (orange)	180	30	127 ± 5
SIA PL731	SIA	Two part (black)	127	30	112 ± 6

sive was supplied by the Automotive Composite Consortium (ACC) and Oak Ridge National Laboratory (ORNL) of the USA as part of the collaborative research programme for the crash analysis of adhesively-bonded structures. The values of the glass transition temperatures, T_g, of the adhesives are also given in Table 1.

Joints were prepared using one of four composite substrate materials, as described in Table 2. Panels of the CFRP materials were prepared according to the manufacturer's recommendations. The first of the composites was manufactured using prepregs of high tensile strength (HTS) carbon fibre and 'HexPly 6376' matrix, supplied by Hexcel (UK), to form unidirectional CFRP panels with a nominal fibre volume fraction of 60%. In the second composite, prepregs of 'T300' carbon fibres supplied by Toray (Japan) and 'HexPly 924' epoxy matrix, produced by Hexcel (UK), were also used to manufacture unidirectional (UD) CFRP panels with a fibre volume fraction of 60%. For the third composite, prepregs of 'IM7' carbon fibres and 'Cycom 977-2' matrix supplied by Cytec Engineered Materials (UK) were used to manufacture unidirectional CFRP panels with a fibre volume fraction of 65%. The final composite was a woven CFRP material, which was supplied by the ACC via Oak Ridge National Laboratory. This material was selected because it readily permits the construction of 'hat sections' and the compression moulding of non-circular tubes with a low variation in thickness and curvature. The material consisted of a '3 K high-tensile plain-weave fabric' in a carbon-fibre epoxy prepreg designated 'ACG MTM 49/CF0501' from Advanced Composites Group (USA) (Starbuck et al., 2004). The resin content in the composite was 42% by weight and the carbon fibre used was 'T300B 40B' from Toray (Japan). Pacific Composites Inc. (USA) produced the orthotropic panels with the configuration presented in Table 2. Such panels are used in the 'PSA Peugeot Citroen Cup 20' car. The values of the flexural moduli, E_1, of the composites are also given in Table 2.

2.2. Joint manufacture

The CFRP substrate panels were cut into beams typically 20 mm wide and 150–180 mm long for the preparation of test specimens. The manufactured panels of the composite substrates were maintained in a vacuum oven at 60 °C until fully dry to ensure that there was no possibility of pre-bond moisture effects being observed in the resulting joints, as has been described in Blackman et al. (2008). The substrates were abraded with 180/220 mesh alumina grit and were cleaned by wiping with an acetone soaked cloth. The adhesive was applied to both surfaces and a bondline thickness of 0.4 mm was always achieved in the joints by the use of wire spacers and/or spherical glass ballotini. The adhesives were cured according to the manufactures' instructions for the two adhesives, as detailed in Table 1.

The joints manufactured for the various fracture tests reported here are listed in Table 3, and are shown schematically in Figs. 1–3. For mode I loading, double-cantilever beam (DCB) test specimens were prepared as detailed in the ISO standard (ISO 2009). These DCB specimens were used for both the quasi-static test rates (designated 'QS' in Table 3) and the high test rates (designated 'H' in Table 3). For mode II loading, the end-loaded split (ELS) and/or the end notch flexure (ENF) test specimens were prepared. The ELS test specimen was only used at quasi-static test rates, but the ENF specimen was used at both quasi-static and high rates. The ELS tests were not performed at high rates due to the likelihood of damaging the test apparatus. For mixed-mode I/II loading, the fixed-ratio mixed-mode (FRMM) and/or the mixed-mode flexure (MMF) test specimens were prepared. The FRMM specimen was only used at quasi-static rates, due again to the likelihood of damaging the test apparatus. However, the MMF specimen was used at both quasi-static and high test rates. Again, the 'QS' and 'H' designations in Table 3 show whether the specimens were used for quasi-static rate (QS), high-rate (H) or for both quasi-static and high-rate tests (QS,H).

2.3. Testing at quasi-static (slow) rates

2.3.1. Quasi-static mode I testing

The DCB specimen is shown in Fig. 1. The testing procedures for quasi-static mode I testing followed the guidelines which are fully described in the international standard, ISO 25217-2009 (ISO 2009). Specimens were precracked in mode I and were then tested at a rate of 1 mm/min using a universal testing machine. Values of the load, P, crosshead displacement, δ, and crack length, a, were recorded during the tests for crack initiation and for steady-state crack propagation. The values of crosshead displacement were corrected for the effects of machine compliance and the values of crack length were measured with the aid of a travelling microscope with a ×10 objective lens. Typically, cracks propagated from a = 50 mm to a = 100 mm during the tests.

2.3.2. Quasi-static mode II testing

For testing at slow rates under mode II loading conditions, the calibrated end-loaded split (C-ELS) (Blackman et al., 2005, 2006) and the end-notch flexure (ENF) test specimens were used. The C-ELS and ENF test specimens are shown in Fig. 2. For either test, the specimens were initially precracked via mode I loading, prior to the mode II test being undertaken.

Table 2
Details of the composite substrates used.

Substrate	Designation	Ply sequence	Thickness, h (mm)	Modulus,[a] E_1 (GPa)
HTS/6376C	HTS	$[0]_{16}$	4	130 ± 5%
		$[0]_{24}$	6	130 ± 5%
T300/924	T300	$[0]_{12}$	3	121 ± 2%
IM7/977-2	IM7	$[0]_{16}$	2	139 ± 3%
Woven	Woven	$[(0/90, \pm 45)_9]_s$	8.5	42 ± 3%

[a] Measured in flexure.

Table 3
The joints investigated at quasi-static test rates (QS) and high-test rates (H).

Joint designation	Sub. thickness, h (mm)	Mode				
		I	II		I/II	
		DCB	ELS	ENF	FRMM	MMF
XD4600 joints						
HTS-XD4600	4,6	QS, H	QS	QS, H	QS	H
T300-XD4600	2	QS, H	QS	QS	QS	QS
IM7-XD4600	3	QS, H	–	–	–	–
Woven-XD4600	8.5	QS, H	QS	QS	QS	–
SIA joints						
HTS-SIA	6	QS, H	QS	QS, H	QS	H
T300-SIA	2	QS	QS	–	QS	QS
Woven-SIA	8.5	QS, H	QS	H	QS	H

(–): Tests not undertaken.

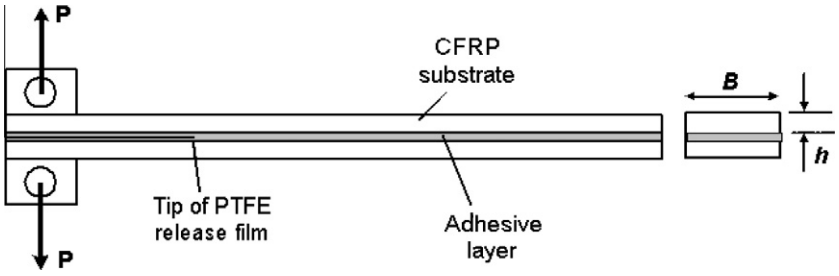

Fig. 1. The mode I DCB adhesive joint test specimen.

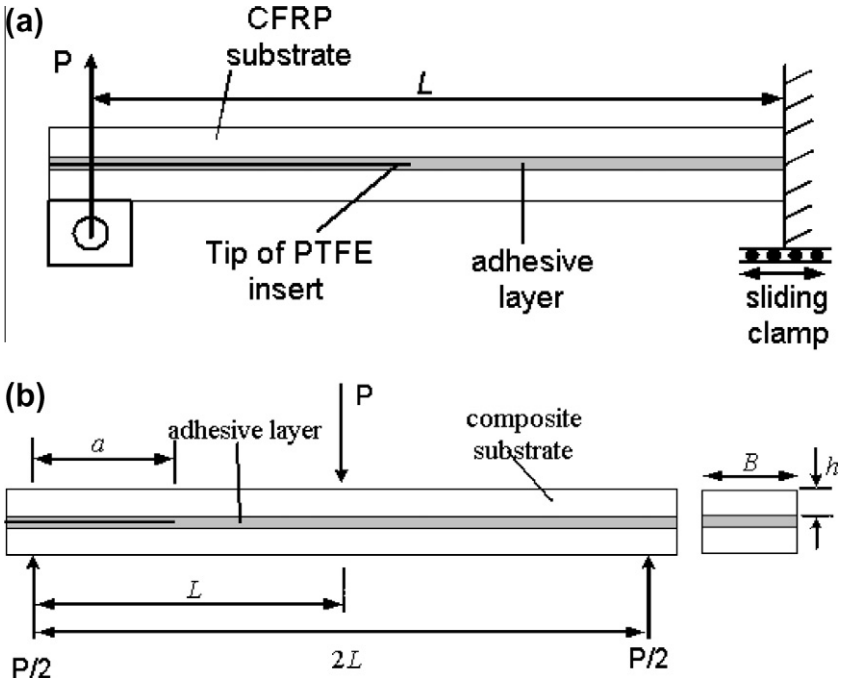

Fig. 2. The mode II adhesive joint test specimens: (a) the calibrated end-loaded split (C-ELS) test specimen and (b) the end-notch flexure (ENF) test specimen.

The C-ELS test required a calibration of the test fixture prior to mode II fracture testing. The calibration was performed using the specimen in the 'inverse configuration' in which the specimen is put into the apparatus with the crack held fully within the clamp, and the specimen was loaded (within the elastic region) for various free lengths, L, from 50 to 100 mm to determine the compliance, C. The procedure has been previously described in detail (Blackman et al., 2005, 2006). The test specimen was then clamped into the mode II ELS test fixture for mode II loading. The clamp fixture was attached to a linear-bearing trolley, which allowed the specimen to slide freely in the horizontal direction during the test. The clamp was tightened to 8 N m to leave the specimen with a known free length in the range $100 < L < 130$ mm, and the specimen was loaded via a load-block mounted on the lower substrate, such that both arms were loaded with equal bending moments. Testing was carried out at a rate of 0.5 mm/min until the crack had propagated

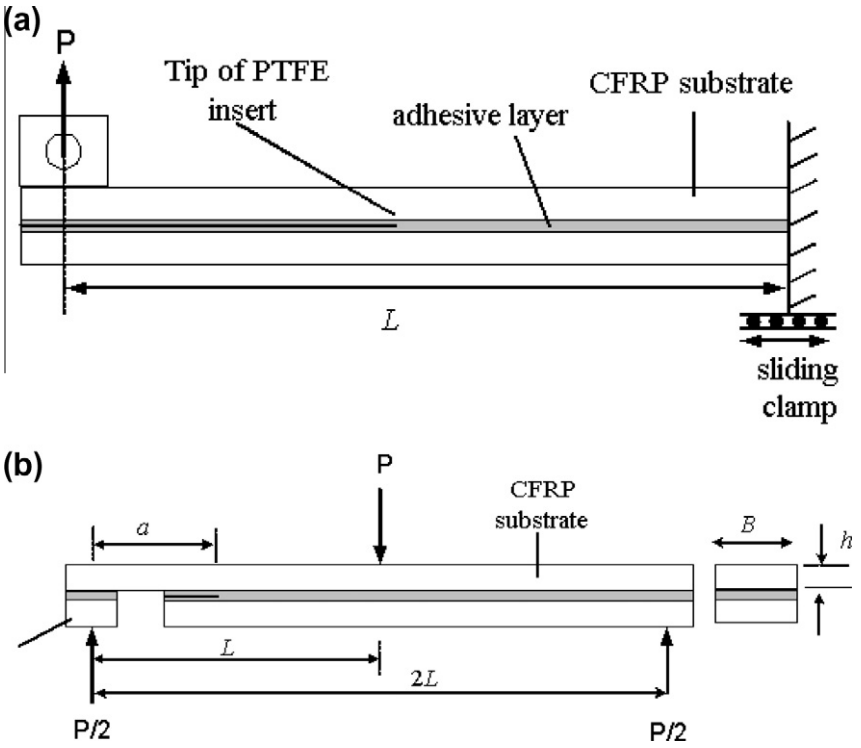

Fig. 3. The mixed-mode I/II adhesive joint test specimens: (a) the fixed-ratio mixed mode (FRMM) test specimen and (b) the mixed-mode flexure (MMF) test specimen.

to within 10 mm of the clamp. Values of load, crosshead displacement and crack length were recorded during the test. The machine compliance and crack lengths were determined as above.

The ENF test used a three-point bending fixture. The diameter of the loading anvils was 10 mm. The support span, $2L$ was set to a value in the range 120 mm < $2L$ < 150 mm and the specimen was positioned such that the initial pre-crack length, $a_p = 0.7L$. Testing was conducted at a rate of 0.5 mm/min and unstable crack propagation always occurred, with the crack propagating instantly to $a = L$ or beyond.

2.3.3. Quasi-static mixed-mode (I/II) testing

For testing at slow rates under mixed-mode I/II loading conditions, the FRMM and the MMF tests were used. The FRMM and MMF specimens are shown in Fig. 3. Both specimens provide an applied mixed-mode ratio, G_I/G_{II}, of nominally 4/3. For either test, the specimens were initially precracked in mode I loading, prior to the mixed-mode I/II test being undertaken.

For the FRMM tests, the test apparatus was the same as used for the C-ELS tests, except that the specimen was loaded via a load block on the upper substrate only and the lower substrate was not loaded. Testing was carried out at a rate of 1 mm/min until the crack had propagated to within 10 mm of the clamp. Values of load, crosshead displacement and crack length were again recorded during the test. The machine compliance and crack lengths were determined as above.

For the MMF tests, the specimen was modified to permit mixed-mode loading to be applied using the same three-point bend fixture as described above. A portion of the lower substrate was carefully cut away and re-attached to the upper substrate at one end, such that the left hand support anvil supported the upper substrate and the right hand support anvil supported the lower substrate. The support span, $2L$ was set to a value in the range 120 mm < $2L$ < 150 mm and the specimen was positioned such that the initial pre-crack length, $a_p = 0.7L$. Testing was carried out at a rate of 1 mm/min and unstable crack propagation always occurred, with the crack propagating instantly to $a = L$ or beyond.

2.4. Testing at high rates

2.4.1. The high-rate test

The high-rate tests were undertaken using a high-speed, open-loop, servo-hydraulic test machine (i.e., an Instron (UK) 'Model VHS') capable of producing a constant displacement rate in tension, or compression, of up to 25 m/s. The position and hence the velocity of the hydraulic ram during the tests was measured using an linear-variable displacement-transducer (LVDT) mounted on the ram. More accurate measurements of specimen displacement and velocity were achieved using high-speed video photography. Two high-speed digital video-cameras were employed: a 'Phantom 4' and a 'Phantom 7.1' camera, both from Vision Research (USA). Both cameras incorporate 8-bit image depth and high sensitivity CMOS sensors. The 'Phantom 7.1' was used for the higher-speed tests, where its faster operational speed was exploited. Frame rates of between 10,000 and approximately 30,000 frames per second (fps) were employed, with exposure times of between 5 and 25 μs. Illumination of the test specimens was achieved via two 1.5 kW flood lights. These provided sufficient illumination for the above exposure times. The lights were controlled to only illuminate immediately prior to the test to avoid specimen heating effects. The load values were measured using a piezo-electric load-cell with a high natural frequency in the range 50–70 kHz. For data and video capture and subsequent analysis, an acquisition system ('Model C2008'), developed by Imatek Ltd. (UK), was used to simultaneously trigger the camera and data acquisition system at a predefined ram position.

2.4.2. High-rate mode I testing

The DCB test specimen was used and the test equipment, as configured for a mode I test, is shown schematically in Fig. 4. The hydraulic ram was operated in the tensile direction. A lost motion

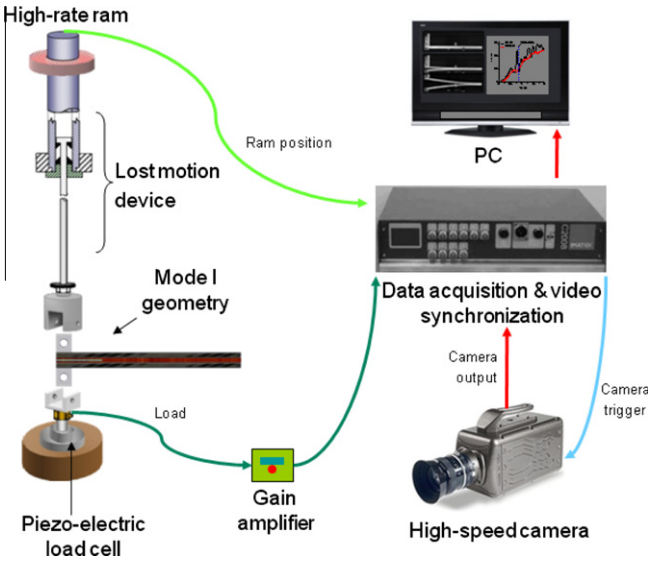

Fig. 4. Schematic diagram of the high-rate test rig, showing the mode I loading arrangement.

device (LMD) was used to couple the hydraulic ram to the upper loading shackle. The purpose of the LMD was to allow the ram to attain a pre-set constant velocity before motion was 'transferred' to the DCB specimen. The shaft of the LMD and shackles were made from titanium alloy to minimise their mass. The LMD incorporated a cup and cone contact unit which allowed the insertion of hard rubber washers to reduce the contact stresses at the instant when the shaft picks-up the specimen. The specimens were initially pre-cracked in mode I at slow rate prior to the high rate DCB test. The DCB specimens were loaded at displacement rates of up to 15 m/s. The high-speed video camera was used to record the motion of the entire specimen during the test. The video records were analysed to obtain the load-line beam opening displacement, the crack length and the crack velocity as a function of time. The procedure used for high-rate testing in mode I has been described previously (Rodriguez-Sanchez, 2008; Blackman et al., 2009).

2.4.3. High-rate mode II testing

The high-rate mode II tests were performed using the ENF test configuration. Fig. 5 shows a schematic view of the high-rate ENF test specimen together with the support fixture and loading anvil. The hydraulic ram was operated in the compressive direction. In this configuration, the load cell was attached directly to the loading anvil. The joints were placed in the fixture so the initial value of the pre-crack length was always given by $a_p = 0.7L$, where $2L$ represents the span between the lower supports, so as to meet the stability criterion (Hashemi et al., 1990). Typically, values in the range $106 < 2L < 131$ mm were used for these tests. Following the recommendations for the three-point bending test at high rates for polymers (ISO 2002), a 5 mm thick visco-elastic pad, of 'Blue Tack' from Bostik (UK), was placed between the striker and the specimen to reduce contact effects. The specimens were initially pre-cracked in mode I at a slow rate prior to the high-rate ENF test. The tests were performed at the nominal ram displacement rates of 0.1 m/s, 1 m/s and 10 m/s. The high-speed video camera was used to record the deformation of one half of the test specimen during the tests. Only the left hand side of the specimen, together with the loading anvil, were recorded in order to optimise the fps and the spatial resolution. With this approach it was possible to obtain a resolution of at least 6 pixels mm^{-1}.

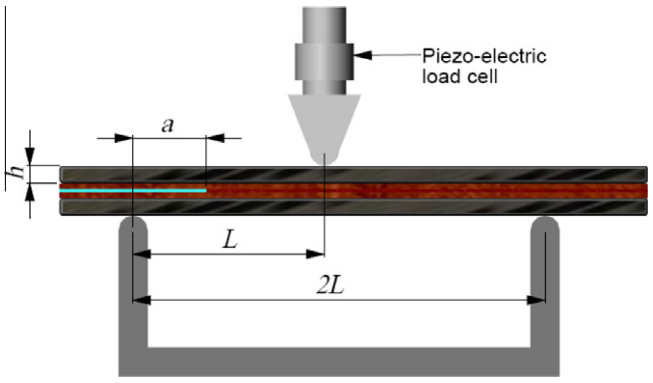

Fig. 5. Schematic diagram of the ENF test specimen used for high-rate testing.

Fig. 6 shows two still images extracted from a high-speed video recording for an ENF test. The displacement, δ, was measured at the mid-span relative to its original position at the instant prior to loading, i.e., at time $t = t_o$. The arrows in the left and right image represent the position in-line with the crack tip. The load-point displacement measured with the LVDT mounted on top of the moving hydraulic ram did not produce reliable measurements of displacement. As observed during the mode I tests, the LVDT measurements did not accurately reflect the true, local deformation of the specimen. Fig. 7 compares the load-point displacement measured in an ENF test for an HTS-XD4600 joint loaded at a nominal test rate of 1 m/s using the LVDT on the hydraulic ram and also using the high-speed video camera. The true displacement and displacement rate of the joint measured via the video camera was always less than that measured by the LVDT. The slower speed of loading actually achieved in the test, as correctly measured by the camera, is most likely to be due to the compression of the visco-elastic damper pad.

2.4.4. High-rate mixed-mode I/II testing

The high rate mixed-mode I/II tests were performed using the MMF test configuration. The hydraulic ram was operated in the compressive direction and the same bending rig, load-cell location and damper pad was used as for the ENF tests described above. The specimens were initially precracked under mode I loading at a relatively slow rate prior to the high-rate MMF test being undertaken. The specimens were positioned so that the initial crack length was given by $a = 0.7L$ and the tests were carried out at the nominal rates of 0.1 m/s, 1 m/s and 10 m/s. High-speed video photography was again used to measure the beam displacement and to detect crack initiation, as described above.

3. Results and discussion: slow-rate, quasi-static tests

3.1. Quasi-static mode I tests

3.1.1. Analysis methods

The quasi-static fracture behaviour observed in the joints under mode I loading was either stable with continuous crack growth (referred to here as 'Type 1' fracture) or was unstable with stick-slip crack growth (referred to here as 'Type 2' fracture). Stable type crack growth occurs when the crack propagates steadily and continuously through the specimen in a stable manner. 'Unstable' is when the crack grows in a stick-slip manner via short bursts interspaced by periods of crack arrest, such that crack initiation and arrest points are visible both in the load versus displacement trace, and on the fracture surfaces. It should be noted that under these slow-rate loading conditions, the effects of kinetic energy are negligible and have therefore been neglected.

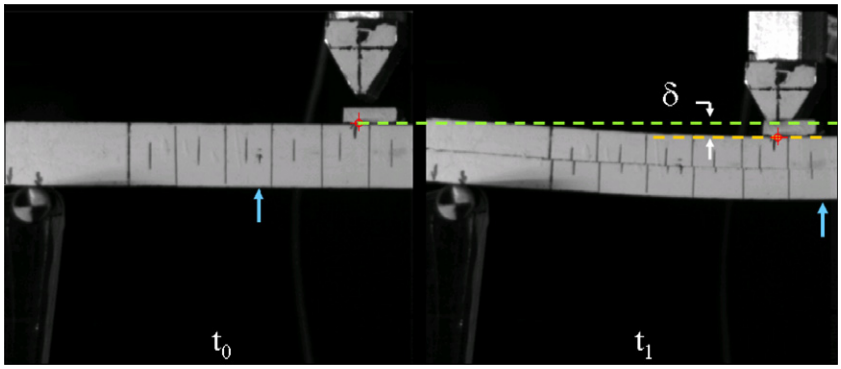

Fig. 6. Two still images extracted from the high-speed video record of an ENF test. (Arrows mark the position of the crack tip. Time $t = t_o$ was prior to loading and time $t = t_1$ was after the crack had propagated past the centre point).

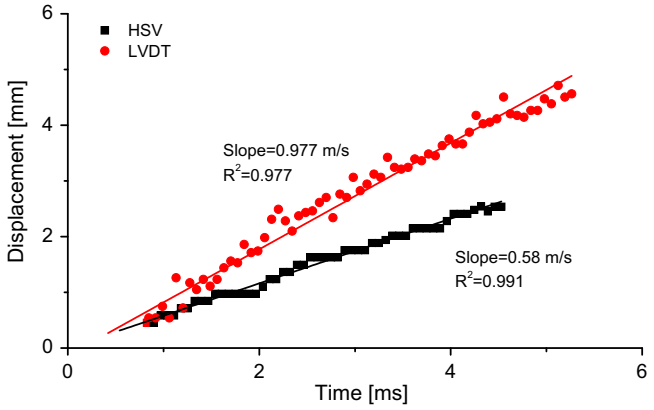

Fig. 7. Graph of mid-point displacement values versus test time for an HTS-XD4600 ENF specimen tested at a nominal rate of 1 m/s. Displacements as measured via the linear-variable displacement-transducer (LVDT) and the high-speed video (HSV) camera are compared.

For the stable continuous, crack growth (i.e., 'Type 1'), the fracture energy was determined via the analysis procedure recommended in the ISO standard (ISO 2009), i.e.:

$$G_{Ic} = \frac{3P\delta}{2B(a+\Delta_I)} \cdot \frac{F}{N} \quad (1)$$

where P is the load, δ the beam opening displacement, B the specimen width, a the crack length. The terms Δ_I, F and N are correction factors, accounting for beam root-rotation and shear effects, large displacements and end-block effects respectively (ISO 2009). For 'Type 1' crack growth, G_{Ic} values were determined using the crack propagation values. For 'Type 2', stick-slip crack growth, Eq. (1) was also used to determine values of G_{Ic}, but only values of crack initiation were used in the calculation. Crack initiation was defined using the max/5% definition (ISO 2009), rather than the non-linear (NL) or visually determined (VIS) definitions of initiation also described in the international standard. The max/5% definition of initiation has been shown to be more repeatable and reproducible, exhibiting less scatter than either the NL or the VIS definitions (Blackman et al., 2003).

3.1.2. Results and discussion

The type of fracture and the nature of the failure path observed for the quasi-static mode I joints are summarised in Table 4. The values of the fracture energy, G_{Ic}, deduced for the different joints are given in Table 4 for crack initiation and for steady-state crack propagation. There are a number of interesting observations.

Table 4
Mode I fracture behaviour and G_{Ic} values for the joints tested at 1 mm/min.

Joint	Failure, anal. type	G_{Ic} (J/m^2)	
		Initiation	PROP.
XD4600 joints			
IM7-XD4600	S/C, 1	3630 ± 7%	3700 ± 5%
T300-XD4600	S/C, 1	3460 ± 5%	3660 ± 6%
HTS-XD4600	S + U*/C, 1	3410 ± 8%	3640 ± 6%
Woven-XD4600	S/D, 1	1390 ± 9%	920 ± 11%
SIA joints			
IM7-SIA	U/C, 2	1860 ± 19%	1890 ± 16%
T300-SIA	U/C, 2	1690 ± 19%	1760 ± 19%
HTS-SIA	U/C, 2	1890 ± 15%	1800 ± 12%
Woven-SIA	U/C + D**, 2	1800 ± 23%	1830 ± 13%

S: stable crack growth; U: unstable crack growth; C: cohesive failure in the adhesive layer; D: delamination of the composite substrate; (*): 2 out of 7 joints showed unstable-cohesive failure; (**): 4 out of 7 tests were cohesive, 3 out of 7 tests exhibited delamination.

Firstly, the values of G_{Ic} at crack initiation and for steady-state propagation are approximately equivalent, showing that there were no significant rising 'R-curve' effects present in the tests under mode I loading. Secondly, it can be concluded that when the failure path was cohesive through the adhesive layer, then the values of G_{Ic} determined for the joints were independent of the substrate material. However, the values were dependent upon the adhesive used, with the XD4600 adhesive being significantly tougher than the SIA adhesive. Thirdly, as might be expected, the values of G_{Ic} were dependent upon the location of the failure path. When the crack grew through the composite substrate, as in the case for the Woven-XD4600 joints, then much lower values of G_{Ic} were determined than when the failure path was cohesive though the adhesive. Fourthly, joints bonded with the SIA adhesive always gave more scatter in the values of G_{Ic} than was apparent in the joints bonded with the XD4600 adhesive. This is suggested to be due to the 'Type 2' fracture (i.e., stick-slip failure) observed in the SIA bonded joints yielding relatively few data points for determining the value of G_{Ic}, compared to 'Type 1' (i.e., stable failure) failure seen in the XD4600 bonded joints which uses many (e.g., typically >15) propagation points.

3.2. Quasi-static mode II tests

3.2.1. Analysis methods

For the slow rate tests at 1 mm/min, both ELS and ENF tests were undertaken to measure the values of G_{IIc} for the joints. Various beam theory and compliance analyses have been developed for the mode II, ELS test specimen. However, analyses which

are dependent upon the measured crack lengths have been shown to be prone to significant errors due to the experimental uncertainty in measuring crack growth in the absence of beam opening displacements (Blackman et al., 2005). Thus, the analysis strategy adopted for quasi-static mode II testing using the ELS specimen followed an effective crack length approach, as outlined in (Blackman et al., 2005). In this approach, the applied load and load-point displacement of the specimen are measured and the effective crack length is determined and used in the analysis. This approach requires an independent measurement to be made of the flexural modulus of the substrate arms and it also requires an experimental calibration to be performed on the ELS fixture, using a test specimen in the so-called 'inverse configuration.' This calibration takes into account the clamping conditions which have been shown to significantly influence the test results (Blackman et al., 2006). The analysis is referred to as the 'Corrected Beam Theory, with Effective Crack Length, (CBTE)' method and the value of G_{IIc} is given by:

$$G_{IIc} = \frac{9}{4}\frac{P^2 a_c^2}{E_1 B^2 h^3} F \tag{2}$$

where P is the load, B is the specimen width, F is the large displacement correction for this loading (Hashemi et al., 1990), E_1 is the flexural modulus of the substrates and h the substrate thickness. The effective crack length, a_c, is given by:

$$a_c = \left[\frac{2Bh^3E_1C}{3N} - \frac{1}{3}(L + \Delta_{clamp})^3\right]^{1/3} \tag{3}$$

where C is the compliance of the beam ($C = \delta/P$) and L is the free length of the specimen in the ELS fixture. The clamp calibration term, Δ_{clamp}, is determined by performing the inverse ELS test using a range of free lengths, and by applying a linear regression to the $C^{1/3}$ versus L data. The value of Δ_{clamp} is given by the negative intercept on the L-axis (Blackman et al., 2005, 2006).

The analysis used for the ENF test follows the corrected beam theory reported in Hashemi et al. (1990), thus:

$$G_{IIc} = \frac{9}{16}\frac{P^2(a + \Delta_{II})^2}{E_1 B^2 h^3} F \tag{4}$$

where Δ_{II} is the correction to the crack length accounting for the effects of beam root-rotation and transverse shear, and the other terms are as defined previously. The ENF tests always exhibited unstable crack growth, so only initiation values of G_{IIc} were deduced using this test method. Thus, only the initial values of crack length were required for the determination of G_{IIc}, so uncertainty in the measurement of crack growth was not a complicating factor in these tests.

The equations presented above can be applied to both 'Types 1 and 2' fracture, recalling that 'Type 1' uses crack propagation values and 'Type 2' uses only crack initiation values to determine G_{IIc}.

3.2.2. Results and discussion

The results for the mode II testing at slow rates are presented in Table 5.

Considering firstly the joints bonded with the XD4600 adhesive, when the substrates were the UD-composites (i.e., the T300 and HTS CFRPs) then the joints failed in a stable manner (i.e., 'Type 1' fracture) in the ELS test, and in an unstable manner (i.e., 'Type 2' fracture) in the ENF test. This observation arises from the well-known effect of the different stability of crack propagation which results from these two different types of test geometry (Hashemi et al., 1990). For all the UD-composites bonded using the XD4600 adhesive, the failure path remained cohesive through the adhesive layer. However, in the case of the Woven-XD4600 joints, then failure in the woven composite substrates occurred at, or very soon after, initiation of the precrack which was located in the adhesive layer. This change of failure path to being via delamination of the composite substrate greatly reduced the values of G_{IIc}, as may be seen from the results shown in Table 5. The joints tested using the ELS test specimen tended to show a strong, rising 'R-curve' behaviour. However, to enable a direct comparison to the results from the ENF test and to the high-rate tests, the G_{IIc} values from the ELS tests in Table 5 have been quoted for crack initiation. Again, for the quasi-static tests, the max/5% definition of initiation has proved to be the most reliable and has been reported here, in preference to the non-linear (NL) or visual (VIS) definitions. The values of G_{IIc} from the ELS test using Eq. (2) are not significantly different in value than those obtained using the ENF test and Eq. (4), which demonstrates that either test could be used to determine the initiation values of G_{IIc}. The initiation G_{IIc} values for the UD bonded composites (i.e., the T300-XD4600 and HTS-XD4600 joints) using the XD4600 adhesive are about 60% higher than their respective mode I initiation values of G_{Ic}, see Tables 4 and 5.

Considering secondly the joints bonded with the SIA adhesive, then these joints tended to exhibit unstable (i.e., 'Type 2') fracture with the failure path being via cohesive fracture within the adhesive layer. The exception was the HTS-SIA joints tested using the ELS test, where stable (i.e., 'Type 1) fracture occurred, with the failure path being cohesive through the adhesive layer. For these joints, which were the only ones for this adhesive tested using both the ELS and the ENF test geometries, excellent agreement between the initiation values of G_{IIc} determined using these two different test geometries was observed. It is noteworthy that the Woven-SIA joints exhibited unstable but cohesive failure, i.e., delamination of the woven-composite substrates did not occur. This intriguing observation is discussed in Section 5 of the present paper, where this observation is explained. For the UD-composites bonded using the SIA adhesive, the initiation values of G_{IIc} were found to be

Table 5
Mode II fracture behaviour and G_{IIc} values at crack initiation (5%/Max definition) for the ELS and ENF tests at 1 mm/min.

Joint	ELS test		ENF test	
	Failure, anal. type	G_{IIc} (J/m^2)	Failure, anal. type	G_{IIc} (J/m^2)
XD4600 joints				
T300-XD4600	S/C, 1	5480 ± 13%	U/C, 2	5180 ± 17%
HTS-XD4600	S/C, 1	5650 ± 8%	U/C,2	5150 ± 6%
Woven-XD4600	S/D,1	3170 ± 15%	U/C, 2	3060 ± 14%
SIA joints				
T300-SIA	U/C, 2	3420 ± 11%	–	–
HTS-SIA	S/C, 1	3280 ± 18%	U/C, 2	3230 ± 27%
Woven-SIA	U/C, 2	2570 ± 14%	–	–

S: stable crack growth; U: unstable crack growth; C: cohesive failure in the adhesive layer; D: delamination of the composite substrate; (–): tests not undertaken.

approximately 80% higher than the corresponding initiation values of G_{Ic} for this joint, see Tables 4 and 5.

3.3. Quasi-static mixed-mode I/II tests

3.3.1. Analysis methods

In the FRMM test, the corrected beam theory expression for the mixed-mode fracture energy, $G_{I/IIc}$, may be written as:

$$G_{I/IIc} = \frac{P^2[3(a+\Delta_I)^2 + 9/4(a+\Delta_{II})^2]}{E_1 B^2 h^3} F \quad (5)$$

where Δ_I and Δ_{II} are the crack length corrections for mode I and mode II loading respectively, and F is the large displacement correction factor (Hashemi et al., 1990). For the MMF test specimen, the corrected beam theory equation is given by:

$$G_{I/IIc} = \frac{P^2[3(a+\Delta_I)^2 + 9/4(a+\Delta_{II})^2]}{4E_1 B^2 h^3} F \quad (6)$$

The equations presented above can be applied to both 'Types 1 and 2' crack growth, as before.

3.3.2. Results and discussion

The mixed-mode I/II results deduced using the FRMM and MMF tests are shown in Table 6 for the various joints tested at a slow rate. These joints always tended to fail in an unstable manner (i.e., 'Type 2' fracture) via delamination in the composite substrates. Those joints tested using both the FRMM and MMF geometries gave very similar results, indicating that either test could be performed with confidence. The $G_{I/IIc}$ results were very dependent upon the substrate material employed, with values ranging from 950 to 2850 J/m^2 when the XD4600 adhesive was employed, and 660–2040 J/m^2 when the SIA adhesive was employed. It is noteworthy that for both adhesives the highest values were measured for the bonded T300 UD-composite substrates.

4. Results and discussion: high-rate tests

4.1. Introduction

The fracture behaviour observed in the joints tested at high rates required some modifications to be made to the analysis strategy (i) to circumvent the problems posed by oscillations in the load traces due to the presence of dynamic effects in the faster tests, and (ii) to account for the kinetic energy associated with the moving specimen arms in the faster tests.

Four analysis types have been previously identified and defined (Blackman et al., 2009).

Now 'Types 1 and 2' fracture have been discussed in the last section and are used to analyse quasi-static fracture progressing in either the stable, steady-state or via the unsteady, stick-slip mechanism, respectively. However, 'Types 3 (fast-rate unstable) and 4 (fast-rate stable)' fracture were then defined and include a correction for kinetic energy, if required, and employ a load-independent analysis route, which has been developed to circumvent the problems in accurately measuring the load when dynamic effects are encountered in the tests. The procedure followed for assessing whether the kinetic energy of the moving specimen arms was significant, and so needed to be corrected for, was to express the energy as a proportion of the total energy release rate and then to compare this value with the quasi-static value of G_{Ic}. If the value associated with the kinetic energy exceeded 5% of the quasi-static value of G_{Ic}, then it was included in the energy balance. If the kinetic energy was <5% of G_{Ic} then it was neglected. Therefore, whether or not to include kinetic energy in the calculations for G_{Ic} depends not only on the test rate and mass of the moving specimen arms, but also upon the fracture energy: a joint bonded with a brittle adhesive will be proportionately more influenced by kinetic energy effects than a joint bonded with a relatively tougher adhesive. As described below, this basic strategy is now applied to the analysis of the fracture data from each of the different modes tested in the present work.

4.2. High rate mode I tests

4.2.1. Analysis methods

At higher test rates the load-independent analysis was followed including the contribution of kinetic energy in the moving arms. To increase the accuracy of the G_{Ic} determination when using either analysis 'Type 2 or 3' for unstable, stick-slip fracture, at least three initiation points were used to determine an average value of G_{Ic}.

For 'Type 3' (fast-rate unstable) crack propagation, the kinetic energy contribution was incorporated into the analysis by assuming that the crack velocity was zero for crack initiation, i.e., $\dot{a} = 0$. To determine whether kinetic energy should be included in the analysis, the ratio of dynamic to static G_{Ic}, i.e., G^d_{Ic}/G^s_{Ic}, was determined. The dynamic value of G_{Ic}, i.e., G^d_{Ic}, is given by (Blackman et al., 1996b):

$$G_{Ic} = G^d_{Ic} = \left[\frac{3}{4}\frac{E_1 h^3 (V/2)^2 t^2}{(a+\Delta_I)^4}\frac{F}{N^2} - \frac{33}{140}\frac{E_1 h (V/2)^2}{c_L^2}\right] \quad (7)$$

i.e.,

$$G^d_{Ic} = G^s_{Ic} - \frac{33}{140}\frac{E_1 h (V/2)^2}{c_L^2} \quad (8)$$

where G^s_{Ic} is the static value of G_{Ic} as determined via Eq. (1) for the DCB test and V is the velocity of loading applied to the DCB arms as measured by high-speed video photography, t, is the test time (i.e., the time from the onset of loading to that required for the initiation of crack growth). The value of Δ_1 is given by the product of the substrate thickness and the constant, χ, such that $\Delta_1 = \chi h$. As χ depends

Table 6
Mixed-mode I/II fracture behaviour and $G_{I/IIc}$ values at crack initiation (5%/Max definition) at 1 mm/min.

Joint	FRMM		MMF	
	Failure, anal. type	$G_{I/IIc}$ (J/m^2)	Failure, anal. type	$G_{I/IIc}$ (J/m^2)
XD4600 joints				
T300-XD4600	U/D, 2	2850 ± 8%	U/D, 2	2510 ± 9%
HTS-XD4600	U/D, 2	950 ± 26%	–	–
Woven-XD4600	U/D, 2	1090 ± 22%	–	–
SIA joints				
T300-SIA	U/D, 2	2040 ± 11%	U/D, 2	2110 ± 11%
HTS-SIA	U/D, 2	660 ± 26%	–	–
Woven-SIA	U/D, 2	860 ± 25%	–	–

S: stable crack growth; U: unstable crack growth; C: cohesive failure in the adhesive layer; D: delamination of the composite substrate; (–): tests not undertaken.

only on elastic properties of the substrate, it will remain relatively constant for the test rates and materials used in this work. An average value of χ was determined from the quasi-static tests for each composite and these values have been used in the analysis of the high rate tests. The term c_L is the longitudinal wave speed in the substrate arms given by:

$$c_L = \sqrt{E_1/\rho_s} \tag{9}$$

The ratio of dynamic to static G, i.e., G^d_{Ic}/G^s_{Ic}, was then determined and if the value of this was less than 0.95, then the kinetic energy correction was considered significant and was taken into account in the analysis. Thus, if:

$$\frac{G^d_{Ic}}{G^s_{Ic}} = 1 - \frac{44}{140}\frac{(a+\Delta_I)^4}{(c_L h t)^2}\frac{N^2}{F} < 0.95 \tag{10}$$

then the dynamic expression for the DCB, i.e., Eqs. (7) and (8) were used to determine the values of G_{Ic}.

For 'Type 4 (fast-rate stable)' crack propagation, the contribution of the kinetic energy was calculated assuming a moving crack was present (i.e., $\dot{a} > 0$). The dynamic expression for G_{Ic} for steady-state crack propagation is given by (Blackman et al., 2009):

$$G_{Ic} = G^d_{Ic} = \left(\frac{3}{4}\frac{E_1 h^3 (V/2)^2 t^2}{(a+\Delta_I)^4}\right)\frac{F}{N^2} - \left(\frac{111}{280}\frac{E_1 h (V/2)^2}{c_L^2}\right) \tag{11}$$

i.e.,

$$G^d_{Ic} = G^s_{Ic} - \frac{111}{280}\frac{E_1 h (V/2)^2}{c_L^2} \tag{12}$$

and it has been assumed here that kinetic energy becomes important when $G^d_{Ic}/G^s_{Ic} < 0.95$, i.e.:

$$\frac{G^d_{Ic}}{G^s_{Ic}} = 1 - \frac{111}{210}\frac{(a+\Delta_I)^4}{(c_L h t)^2}\frac{N^2}{F} < 0.95 \tag{13}$$

When this condition is met, the dynamic expression for the DCB, i.e., Eqs. (11) and (12), were used to determine the values of G_{Ic}. The values of a, V and t were measured from an analysis of the high-speed digital video recordings. The crack length correction Δ_I was determined as for fracture 'Type 3', described above.

It should be noted that distinguishing between stick-slip and stable crack growth is not always simple in high-rate testing, since the frequency of the stick-slip cycle tends to increase with increasing rate, making a high rate stick-slip fracture sometimes appear to be apparently stable. In the present work, the distinction between stick-slip and stable, continuous crack propagation has been made by performing a linear regression of the a versus $t^{1/2}$ data (Blackman et al., 2009). Stable, steady-state crack propagation is linear with root time for the DCB specimen (Blackman et al., 1995, 1996a), so any departure from this behaviour was assessed. This was achieved by ascertaining the correlation coefficient, R^2, to the regression data. If $R^2 > 0.95$, then the test was considered stable and has been classified as being 'Type 4 (fast-rate stable)'. If $R^2 < 0.95$, then the test was considered unstable and was classified as being 'Type 3 (fast-rate unstable)'. Now, the crack velocity may be determined from the slope to a graph of crack length versus time. For 'Type 4 (fast-rate stable)', and of course 'Type 1 (slow-rate stable fracture), this procedure is accurate. However, for 'Type 3 (fast-rate unstable)' fracture, such an approach yields an average crack velocity over the various stick-slip jumps observed in the tests. Thus, for fracture 'Type 3', and indeed 'Type 2' fracture, the crack velocity determined is referred to as the 'event averaged crack velocity' and represents only an approximation to the true crack velocity in these tests.

Table 7
High rate mode I fracture behaviour.

Joint designation	Failure, anal. type		
Rate m/s:	0.1	1.0	10.0
XD4600 joints			
HTS-XD4600	U/C, 2	U/C, 2	S/C, 4
T300-XD4600	–	–	–
IM7-977-2	U/C, 2	U/C, 2	–
Woven-XD4600	S/D, 1	S/D, 1	S/D, 4
SIA joints			
HTS-SIA	–	U/C, 3	S/C, 4
T300-SIA	–	–	–
Woven-SIA	U/C, 3	U/C, 3	S/C, 4

S: stable crack growth; U: unstable crack growth; C: Cohesive failure in the adhesive layer; D: delamination of the composite substrate; (–): tests not undertaken.

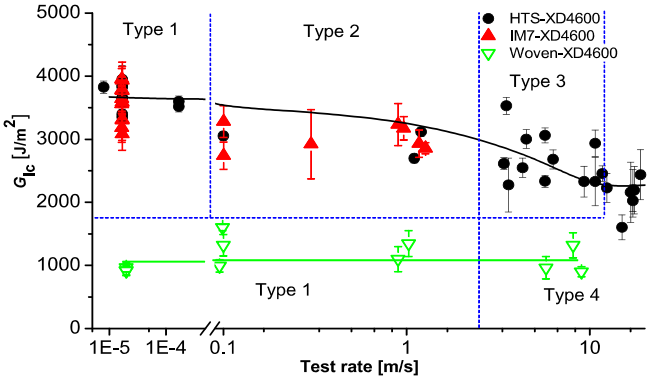

Fig. 8. Values of G_{Ic} versus test rate on logarithmic scale for the DCB joints bonded with the XD4600 adhesive. (Values represent mean propagation values for Fracture Types 1 and 4 or mean initiation values for Fracture Types 2 and 3. Filled symbols represent cohesive failure in the adhesive and open symbols composite delamination.)

4.2.2. Results and discussion

A summary of the mode I fracture behaviour is given in Table 7. The values of G_{Ic} as a function of test rate for the joints bonded with the XD4600 adhesive are shown in Fig. 8 for the various different composite substrates. Also shown in Fig. 8 are the boundaries between the different fracture types, and hence the different analysis methods applicable to each region of the graph, are shown. It was apparent from an inspection of the fracture surfaces of the joints that those prepared with the UD-composite (HTS or IM7) substrates failed in an entirely cohesive manner, i.e., within the adhesive layer, whereas those prepared with the woven CFRP substrates failed by delamination in the composite arms. The different failure paths observed in the UD and the woven joints was consistent with the observation that the measured values of G_{Ic} were always lower for the woven joints when compared to either of the UD composites. The reasons for the different failure paths being observed are discussed further in Section 5 of the present paper. Fig. 9 shows the values of G_{Ic} for the joints bonded with the XD4600 adhesive, but now with the values plotted against crack velocity. Figs. 10 and 11 shows the results obtained for the joints bonded with the SIA adhesive. Fig. 10 shows the values of G_{Ic} versus the rate of test, and Fig. 11 plots these values as a function of crack velocity. For the joints bonded with the SIA adhesive, the slow rate tests all exhibited cohesive but unstable (stick-slip) crack propagation, i.e., 'Type 2' or 'Type 3' fracture. The results show a similar trend to the results reported by Dillard et al. (2011) who investigated the mode I fracture resistance of joints bonded with the SIA adhesive with various substrates using a driven wedge technique.

As was discussed in Blackman et al. (2009), the limitations of the test rate and crack velocity parameters led to a search for a

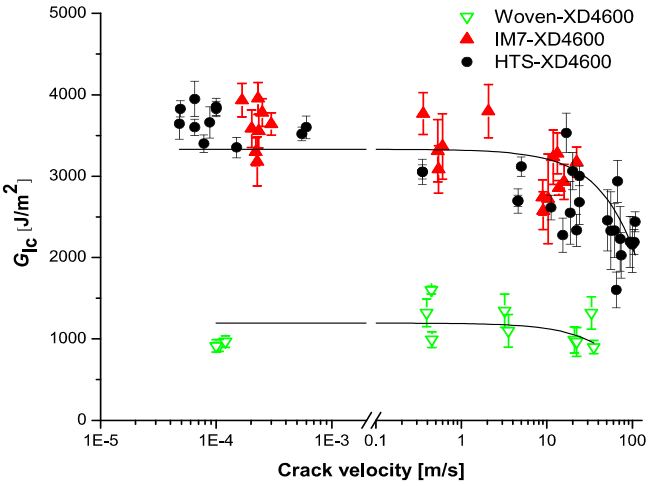

Fig. 9. Values of G_{Ic} versus crack velocity on logarithmic scale for the DCB joints bonded with the XD4600 adhesive. (Values represent mean propagation values for Fracture Types 1 and 4 or mean initiation values for Fracture Types 2 and 3. Filled symbols represent cohesive failure in the adhesive and open symbols composite delamination.)

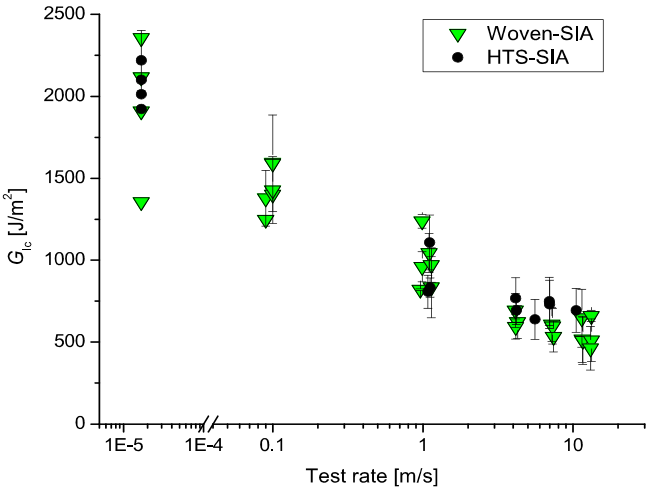

Fig. 10. Values of G_{Ic} versus test rate for joints bonded with the SIA adhesive. (Circles: HTS substrates; Triangles: Woven substrates).

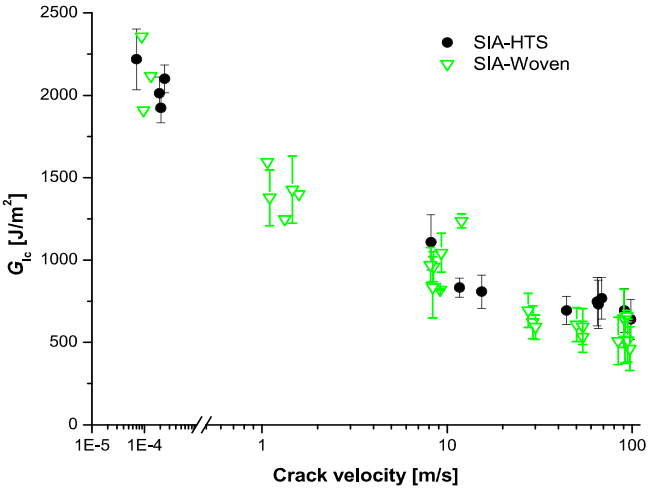

Fig. 11. Values of G_{Ic} versus crack velocity for joints bonded with the SIA adhesive. (Triangles: Woven composite, Circles: HTS composite).

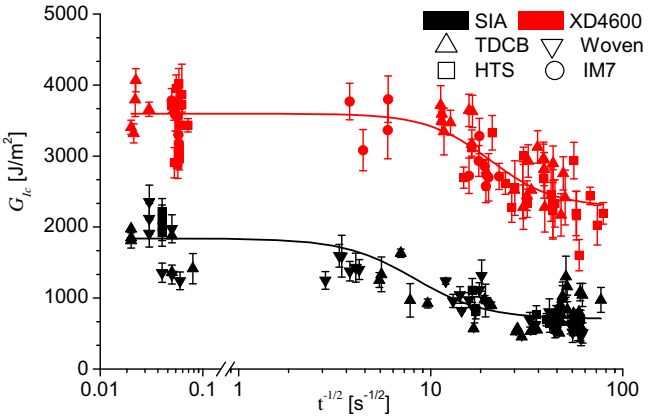

Fig. 12. Comparison of the values of G_{Ic} vs $t^{-1/2}$ for joints bonded with either the XD4600 or the SIA adhesive.

more appropriate and meaningful parameter against which to plot the values of G_{Ic} for the joints. According to thermodynamic arguments, the parameter $t_i^{-1/2}$ was shown to yield consistent results based upon the occurrence of an adiabatic-isothermal transition, leading to the thermal softening of the adhesive at higher test rates, where t_i is the time from the onset of loading to crack initiation. The results for both adhesives are now given in Fig. 12, with the values of G_{Ic} plotted as a function of the time parameter, $t_i^{-1/2}$. This parameter was shown to accurately describe the thermal softening behaviour of the adhesives according to the adiabatic heating model proposed in Blackman et al. (2009). In this model, the time taken is the time to first crack initiation, and the lines drawn on the graph to model both the XD4600 and the SIA adhesive correspond to a thermally affected strip of thickness 25 μm and 1 μm in size, respectively (Blackman et al., 2009). As may be seen, for both adhesives the adiabatic-isothermal model is in good agreement with the experimental results. The data shown in Fig. 12 relate to cohesive failure in the adhesive only. Those tests where delamination occurred are not included in Fig. 12, i.e., the woven-XD4600 values are not included, but the woven-SIA values are. Also show on Fig. 12, for comparison, are values of G_{Ic} determined using the tapered double cantilever beam (TDCB) test with tapered substrates made from aluminium alloy and bonded using either the XD4600 or the SIA adhesive. The TDCB tests and results for the XD4600 adhesive have been reported previously (Blackman et al., 2009; Karac et al., 2011). The values relate to cohesive failure in the adhesive, and excellent agreement was shown when these values were compared to values obtained from DCB tests, for a given value of t_i.

4.3. High rate mode II tests

4.3.1. Analysis methods

As noted above, both the ELS and the ENF tests were used at slow rates of test, but only the ENF test was used at high rates. The effects of kinetic energy were determined to be negligible for the test rates employed and therefore did not affect the G_{IIc} values determined, i.e., the values of G_{IIc}^d/G_{IIc}^s were always greater than 0.95. The high-rate ENF test results were analysed using a load-independent analysis method, given by:

$$G_{IIc} = G_{IIc}^d = \frac{36(a+\Delta_{II})^2\delta^2 E_1 h^3}{[3(a+\Delta_{II})^3 + 2L^3]^2}F \tag{14}$$

where δ is the load-point displacement, a the crack length, E_1 the flexural modulus of the substrate, h the substrate thickness, L the half span, and Δ_{II} and F are the correction factors for beam

root-rotation and transverse shear and for large displacements, respectively (Hashemi et al., 1990). At high rates, the load traces were influenced by dynamic effects. These effects introduced significant non-linearities into the load traces, significantly complicating the determination of the 5% offset initiation point. Hence in these fast-rate tests, the onset of crack initiation was determined using a visual definition, as determined from an analysis of the high-speed video records.

4.3.2. Results and discussion

Crack initiation from the high rate ENF tests was always unstable, with the crack growing immediately to the central loading point. The mode II tests performed always resulted in cohesive failure within the adhesive layer at the initiation of crack growth. Fig. 13 shows the load-versus time traces recorded for ENF tests at three different test rates. The locations of the crack initiation points, as detected by the high-speed video analysis, are shown by the arrows in Fig. 13. The traces shown in Fig. 13 demonstrate the severity of the dynamic effects present at the loading rate of 10 m/s and illustrate that it was not sensible to try to determine the instant of crack initiation from an inspection of the load traces. As can be seen, there was no clear, characteristic feature on the load traces associated with crack initiation. However, detecting the initiation point was quite straightforward on the high-speed video records. The arrows on the traces in Fig. 13 indicate the instant of crack initiation, as determined using high speed photography.

Fig. 14(a) shows a sequence of ten video stills taken from the high speed video records during a test at 0.6 ms. Image 1 was recorded at the instant when the first displacement was recorded on the test specimen following some initial compression of the damper by the striker. Images 1–9 were recorded at a frame interval of 0.36 ms, during which time the crack initiated and grew past the central loading point. Image 10 was taken after the final failure of the substrate. The elapsed time for frames 1–9 is indicated by the vertical dashed lines on Fig. 14(b), together with the measured values of the load (from the load-cell) and displacement (from the high speed video). The white arrows on the video stills identify the position of the crack tip as seen in the video record. It extends past the known initial crack length (i.e., it initiates) between frames 5 and 6 in this sequence. It should be noted that only a sample of the total number of frames recorded are shown in Fig. 14. Fig. 14(c) shows the measured load values up to and past the point of final substrate failure, as indicated by the final video still. When the values of G_{IIc} were deduced for crack initiation for the various test rates employed, then when the load-independent analysis method was used (Eq. (14)), the values remained relatively insensitive to the applied test rate, as can be seen in Table 8. If the load-dependent analysis had been used (Eq. (4)), then the values of G_{IIc} would have shown a strongly increasing trend with test rate, as shown in Fig. 15. This would have led to the erroneous conclusion that the fracture energy, G_{IIc}, in mode II increased with increasing test rate.

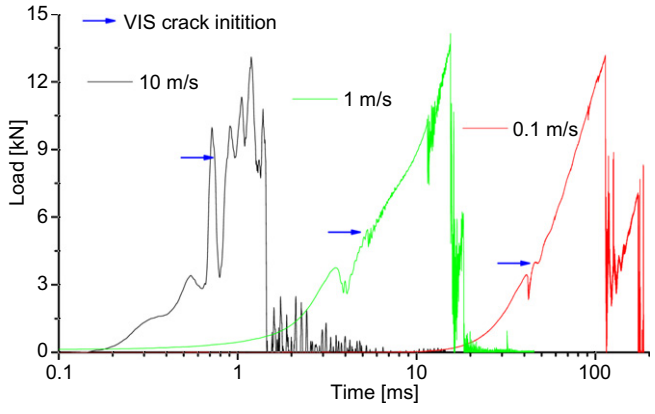

Fig. 13. Load versus time plots (log scale) for HTS-SIA joints tested with the ENF geometry ($2L$ = 131 mm, a = 46 mm). The arrows show the crack initiation point as determined using the HSV analysis.

4.4. High rate mixed-mode I/II tests

4.4.1. Analysis methods

As noted above, the FRMM test geometry was used only for the slow-rate tests. However the MMF geometry was used at both slow and high rates. The effects of kinetic energy were determined to be negligible for the test rates employed and were therefore not included in the analysis, i.e., the values of $G^d_{I/IIc}/G^s_{I/IIc}$ were always greater than 0.95. The high-rate MMF test results were analysed using a load-independent analysis method, given by (Rodriguez-Sanchez, 2008):

$$G_{I/IIc} = G^d_{I/IIc} = \frac{[3(a+\Delta_I)^2 + \frac{9}{4}(a+\Delta_{II})^2]\delta^2 E_1 h^3}{[7(a+\Delta_{II})^3 + L^3]^2} \cdot F \tag{15}$$

where the terms have all been defined previously. Eq. (15) can be partitioned into the individual mode I and II components of G_c, noting that the ratio G_{Ic}/G_{IIc} = 4/3.

4.4.2. Results and discussion

The mixed-mode tests performed on the HTS-XD4600 and the HTS-SIA joints always failed by unstable crack propagation occurring via delamination in the composite substrate. Fig. 16 shows still images extracted from the high-speed video record of an HTS-SIA joint tested at 1 m/s. The image at t = 5 ms is just prior to crack initiation. At t = 10 ms, the crack has propagated in an unstable manner, within the first few plies of the upper composite substrate. At t = 20 ms, transverse fracture of the substrate has occurred.

When the values of $G_{I/IIc}$ were deduced using the load-independent analysis approach (Eq. (15)), then the values deduced were relatively insensitive to test rate as shown in Table 9. However, when a load-dependent analysis was employed (Eq. (6)), then the values of $G_{I/IIc}$ increased strongly with increasing test rate. Again, as discussed previously for the mode II results, this would have been an incorrect conclusion and would have resulted simply from the dynamic effects present in the test. As the values of $G_{I/IIc}$ deduced were associated with the crack running through the composite substrate, then the values obtained were much lower than were measured in the other test modes, when cohesive failure within the adhesive layer was observed. Indeed, the values obtained were characteristic of delamination failure within the composite. The values of $G_{I/IIc}$ deduced are summarised in Table 9, as a function of test rate for the HTS-XD4600 and the HTS-SIA joints. It is clearly of interest to determine why the joints with composite substrates failed in a cohesive manner (within the adhesive layer) when either mode I or mode II loading was applied, but tended to fail via an interlaminar fracture path when mixed-mode loading was applied. This observation appeared to be independent of the test rate. The crack failure paths in the various joints are discussed in Section 5.

5. Results and discussion: the failure loci of the joints

5.1. Effect of test rate

The failure locus for the joints bonded with the XD4600 adhesive is shown in Fig. 17 for the tests conducted at the slow rate

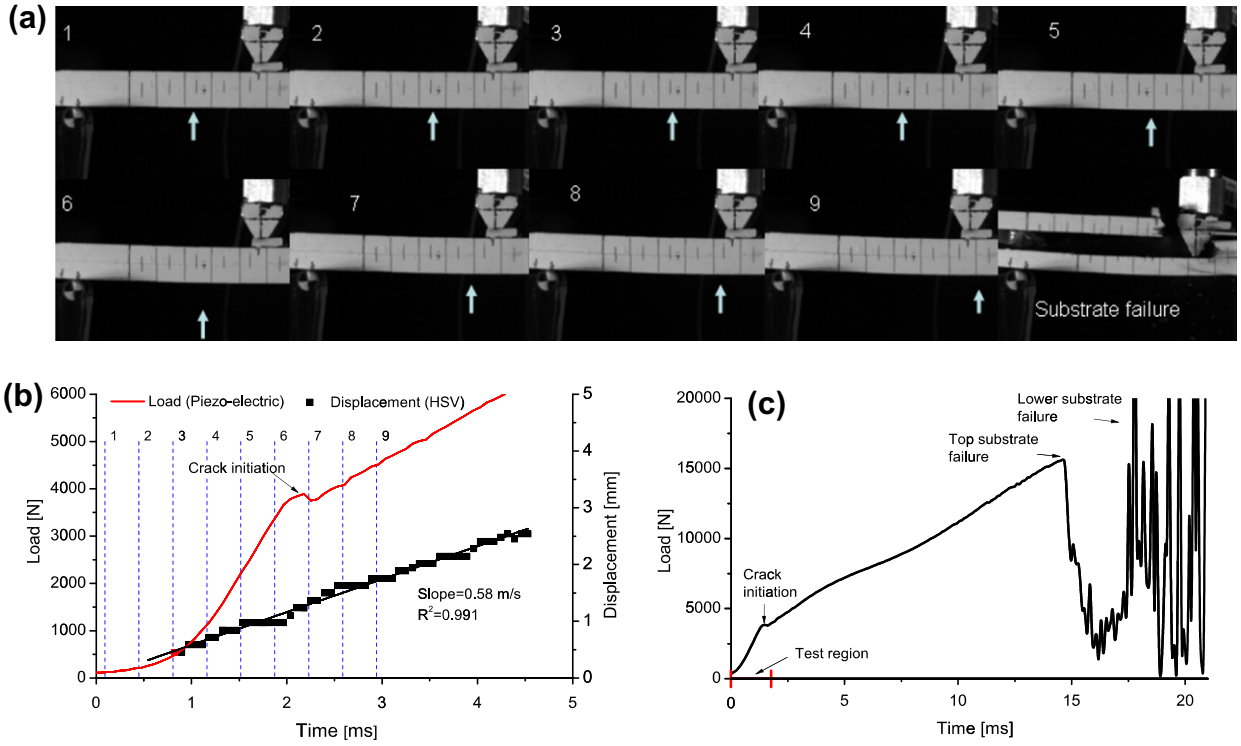

Fig. 14. Results of an ENF test on the HTS-SIA joint tested at 0.6 m/s. (a) Sequence of ten stills from the high speed video record of the test at a frame interval of 0.36 ms. (b) Load (piezo-electric load cell) and displacement (HSV) versus time; (c) full view of load trace showing points of crack initiation and substrate failure. (The dashed lines in (b) correspond to the video images 1–9 from (a)).

Table 8
Summary of the failure paths, analysis types and G_{IIc} values from the mode II tests, as a function of test rate.

Joint	G_{IIc} (initiation) J/m^2					
Geometry:	ELS	ENF				
Rate:	1 mm/min	1 mm/min	0.1 m/s	1 m/s	5 m/s	10 m/s
HTS-XD4600	5650 ± 8% S/C, 1	5150 ± 6% U/C, 2	4010 ± 8% U/C, 2/3	4060 ± 10% U/C, 3	4300 ± 9% U/C, 3	4600 ± 10% U/C, 3
HTS-SIA	3280 ± 18% S/C, 1	3230 ± 27% U/C, 2	3130 ± 12% U/C, 2	3170 ± 10% U/C, 3	3130 ± 11% U/C, 3	3100 ± 12% U/C, 3

S: stable crack growth; U: unstable crack growth; C: cohesive failure in the adhesive layer; D: delamination of the composite substrate.

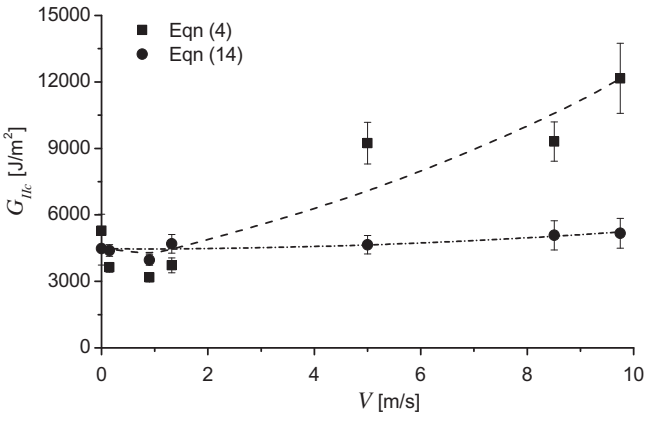

Fig. 15. Values of G_{IIc} (visual initiation) versus test rate for the ENF tests on the HTS-XD4600 joints. Square symbols refer to the load dependent CBT analysis (Eq. (4)) circular symbols to load independent 'LID analysis' (Eq. (14)).

of 1 mm/min. For pure modes I or II loading the failure paths were fully cohesive for the T300 or HTS composite substrates and the values of G_c deduced were independent of which composite was used to make the joint. The value of G_{IIc} for crack initiation was in the range 5150–5650 J/m^2, being approximately 1.6 times the initiation value for G_{Ic}. However, the joints loaded in mixed-mode ($G_I/G_{II} = 4/3$) failed via a delamination mechanism, with the crack switching from the position of the cohesive pre-crack to a path within the composite substrate. Under these conditions the mixed-mode value of G_c was dependent upon the composite substrate, with the joints formed with the HTS composite substrates exhibiting a significantly lower G_c values than the joints with the T300 composite substrates. It is believed that this difference depends more on the transverse tensile strength of the composite (which controls its propensity to delaminate) than on the interlaminar G_{Ic} value of the composite (this will be discussed in more detail in the next section). Whilst various mixed-mode failure criteria have been proposed for cohesive fracture in adhesive joints, these criteria are not appropriate for the situation when

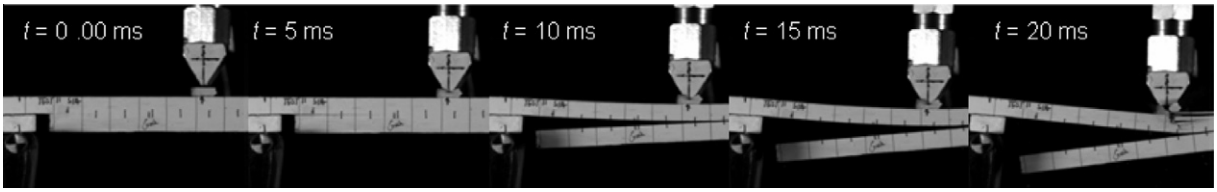

Fig. 16. Still photographs from the HSV for a MMF HTS-SIA joint tested at 1 m/s.

Table 9
Summary of the failure paths, analysis types and $G_{I/IIc}$ values from the mixed-mode tests as a function of test rate.

Joint	$G_{I/IIc}$ (initiation) J/m^2					
Geometry:	FRMM	MMF				
Rate:	1 mm/min	1 mm/min	0.1 m/s	1 m/s	5 m/s	10 m/s
HTS-XD4600	950 ± 26% U/D, 2	– –	640 ± 3% U/D, 3	650 ± 4% U/D, 3	700 ± 5% U/D, 3	750 ± 5% U/D, 3
HTS-SIA	660 ± 26% U/D, 2	– –	660 ± 6% U/D, 3	670 ± 5% U/D, 3	690 ± 5% U/D, 3	710 ± 7% U/D, 3

S: stable crack growth; U: unstable crack growth; C: Cohesive failure in the adhesive layer; D: delamination of the composite substrate; (–): tests not undertaken;

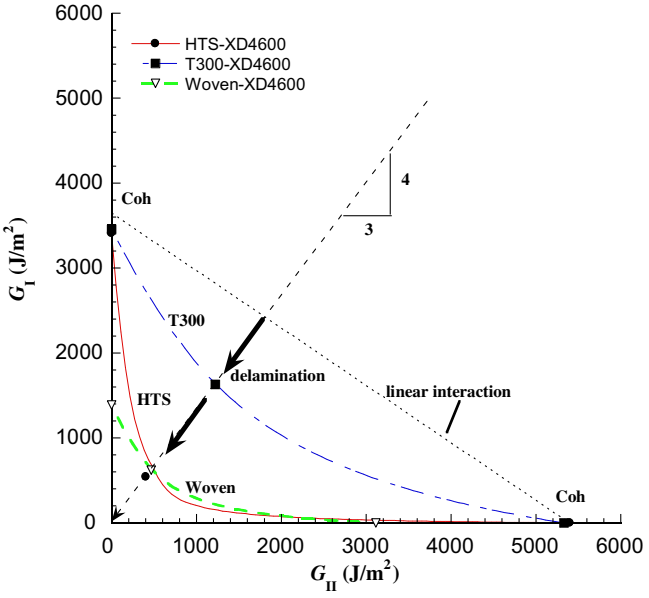

Fig. 17. Failure locus for the joints bonded with the XD4600 adhesive at 1 mm/min.

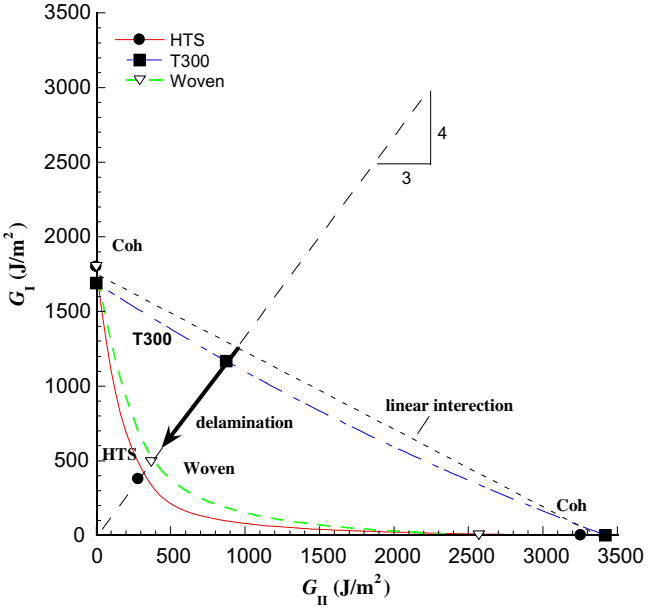

Fig. 18. Failure locus for the joints bonded with the SIA adhesive at 1 mm/min.

the failure path switches from cohesive in the adhesive to the delamination of a composite substrate. A linear interaction line is depicted on Fig. 17 for reference and it is clear that such criteria are unable to accurately describe the mixed-mode fracture behaviour observed in the present work. The joints employing the woven composite substrates exhibited different behaviour. These joints exhibited a delamination fracture path in the pure modes, in addition to mixed-mode. Thus, for this joint system, there was not a change in the fracture path, the value of G_{IIc} was about 3100 J/m^2, G_{Ic} was about 1390 J/m^2, such that the multiple was 2.2 times and the failure locus was closer to that of a linear interaction, but not sufficiently close for this to be an accurate description.

Turning now to the joints bonded with the SIA adhesive and tested at the slow rate of 1 mm/min, the failure locus is plotted in Fig. 18. Whilst the values of G_{Ic} and G_{IIc} are lower for these joints, as the cohesive toughness of the adhesive is now lower than XD4600, the data follow a broadly similar trend to those observed in Fig. 17. Again, the mixed-mode values of G_c are dominated by the effect of delamination and again the effect is greatest for joints when bonding the HTS composite, where the lowest values of G_c were measured in mixed-mode. It is noteworthy that the joints bonding the woven composite substrates did not now delaminate under mode I loading as was observed when bonding this composite with the tougher, XD4600 adhesive. This observation is discussed further in Section 5.2.

Fig. 19 shows the effects of test rate on the G_c values for the HTS composite substrates bonded with the XD4600 adhesive. A reduction in G_c was observed for both the pure modes of loading as the rate was increased from 1 mm/min to 10 m/s. However, this rate effect was relatively small compared to the effects of composite delamination, which always occurred when the joints were loaded in mixed-mode. Similar results were observed for the joints bonded with the SIA adhesive as shown in Fig. 20. Under mixed-mode loading, whilst the effects of rate are negligible, the effects

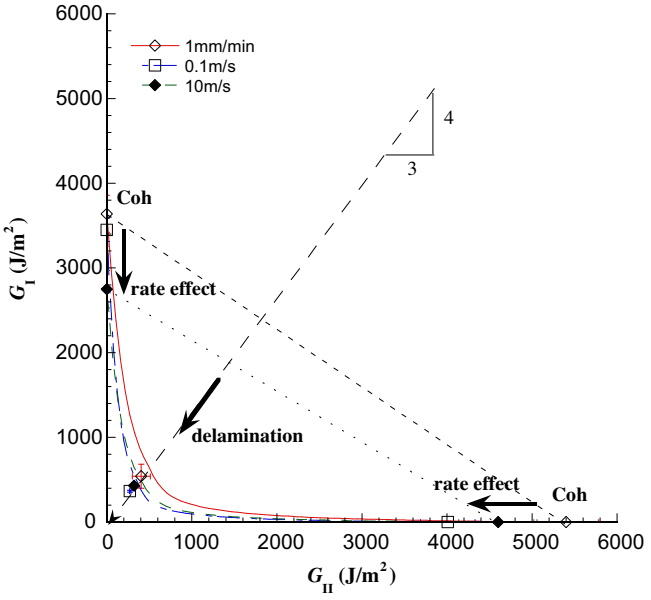

Fig. 19. Failure locus for the joints bonded with the XD4600 adhesive as a function of test rate.

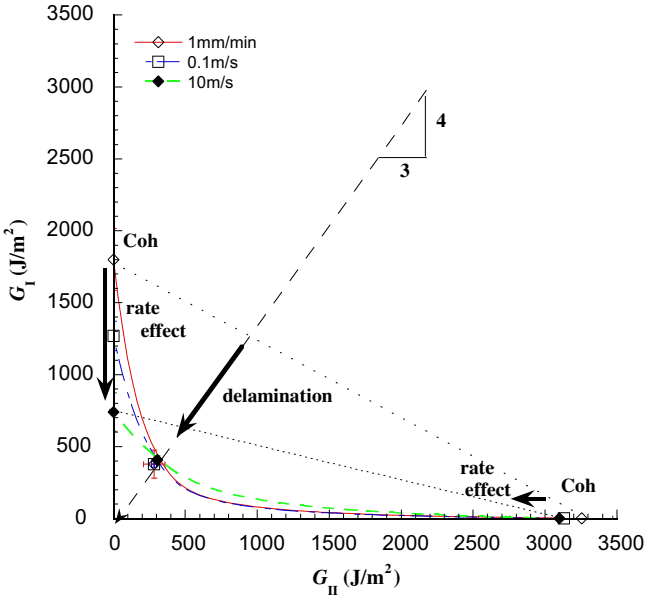

Fig. 20. Failure locus for the joints bonded with the SIA adhesive as a function of test rate.

of delamination are significant. This adhesive however, showed a much greater sensitivity to test rate in mode I than was observed for the XD4600 adhesive: the cohesive value of G_{Ic} fell from 1800 J/m^2 at 1 mm/min to about 730 J/m^2 at 10 m/s. The mode II sensitivity to test rate appeared to be much smaller, as G_{IIc} was almost independent of test rate over the range 1 mm/min to 10 m/s. When composite delamination occurred, i.e., in mixed-mode, then no effects of test rate were evident in the values of G_c deduced. It is clearly noteworthy that the values of G_{Ic} appear to be more rate sensitive than the values of G_{IIc}. Both failures were fully cohesive, so this points to the toughening mechanisms which operate in the rubber modified adhesives being more rate sensitive in mode I than in mode II. Further, as noted by Sun et al. (2009a), the mode II fracture behaviour did not exhibit the transitions that were observed in mode I. These transitions were summarised in Table 8 for the high rate ENF tests and show that only unstable, cohesive crack growth was observed (analysis Types 2 and 3) whereas in mode I, transitions from stable to unstable and back to stable (analysis Types 1–4) were observed.

5.2. Modelling the failure loci

5.2.1. Introduction

Laminated composites, such as those studied in this work, exhibit high strength and stiffness in the fibre direction but can be weak in the transverse directions due to the directionality of the reinforcement. In the results presented previously, some of the joints, especially those loaded in mixed-mode, failed by a crack initiating and then growing in the composite substrate. It was noticed that a crack initiated in the composite substrate, close to the interface with the adhesive, typically one lamina above the interface, and almost in line with the original pre-crack. Subsequent loading caused these cracks to join and then propagate in the composite. When this behaviour was observed, significantly lower values of the fracture energy, G_c, were deduced. With similar adhesive joints systems, it has been shown that this type of failure is related to the transverse properties of the composite (Kinloch et al., 1992), in particular, to the transverse tensile strength, σ_{yyc}. In this section, a simple model to evaluate the likelihood of the composite delamination in adhesive joints is presented.

5.2.2. The composite delamination model

The interlaminar fracture model proposed by Williams (1988) describes the fracture energy not in terms of a local stress field but in terms of the global bending moments applied to the specimen. Using this analysis and the assumptions that (i) fracture is very local and (ii) that the deformation can be modelled as a beam on an elastic foundation, the stresses imposed on the composite substrates during the different in-plane loading modes I, II and I/II can be calculated. Fig. 21 shows the coordinate system followed.

For mixed-mode loading at any test rate, an approximation to the cohesive value of fracture energy for the joints, $G_{I/IIc}$ may be obtained by linearly interpolating between the cohesive values of G_{Ic} and G_{IIc}. A linear interaction parameter k can be defined as:

$$G_{IIc} = kG_{Ic} \tag{16}$$

and then the stresses induced in a *single* composite-substrate arm may be expressed only in terms of the values of G_{Ic} for cohesive failure in the adhesive, and on the substrate properties. The transverse stress, σ_{yy}, on a *single* composite-substrate arm (Williams, 1989; Williams and Hadavinia, 2002) for the three different loading modes investigated here can be expressed as:

$$\text{For mode I loading}: \quad \sigma_{yy} = \frac{2}{\chi^2}\alpha_I\sqrt{\frac{E_1 G_{Ic}}{h}} \tag{17}$$

$$\text{For mode II loading}: \quad \sigma_{yy} = \frac{2}{\chi^2}\alpha_{II}\sqrt{\frac{E_1 G_{Ic}}{h}} \tag{18}$$

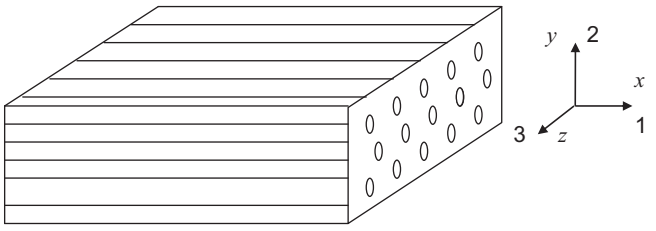

Fig. 21. Co-ordinate system employed for the composite materials.

$$\text{For mixed-mode loading}: \quad \sigma_{yy} = \frac{2}{\chi^2}\alpha_{I/II}\sqrt{\frac{E_1 G_{Ic}}{h}} \tag{19}$$

where

$$\alpha_I = \frac{1}{\sqrt{12}}, \quad \alpha_{II} = \frac{\sqrt{k}}{3}, \quad \alpha_{I/II} = 2\left(\frac{k}{9+12k}\right)^{1/2} \tag{20}$$

and where χ is the crack length correction constant which includes the effect of crack tip rotation and deflection, as defined previously. The values of χ for the composite substrates have been obtained experimentally from the quasi-static tests on the joints, as described previously. The values obtained and used in the analysis are summarised in Table 10. For each substrate, somewhat higher values of χ were obtained when bonding the XD4600 adhesive than when bonding the SIA adhesive. Eq. (19) is only valid for a G_{Ic}/G_{IIc} ratio of 4/3, as used in the present work, however, other mixed-mode ratios would be simple to accommodate using this scheme.

Table 10 additionally shows the measured values of the transverse tensile strength, σ_{yyc} for the various unidirectional composites according to procedure described in ASTM D3039 (ASTM 2007). Rectangular specimens 150 mm long and 20 mm wide, with the fibres aligned at 90 degrees with respect to the loading direction, were tested in tension. These measurements assumed that the transverse tensile strengths of the unidirectional composites were the same in the two perpendicular directions to the reinforcement direction (i.e., $\sigma_{yyc} = \sigma_{zzc}$). A somewhat different procedure was needed for the woven composite. In this case, the transverse tensile strength was measured by loading square sections (25 mm × 25 mm) of the woven composite which had been bonded between aluminium tabs and loaded in tension to failure (Teo, 2008). Table 10 gives the mean and standard deviation values obtained for three repeat tests on each composite substrate. The values of σ_{yyc} quoted in manufacturer's data sheets are also shown for comparison, when available. The experimental values tend to be somewhat lower than those quoted, probably due to the processing conditions used. The results shown for the HTS composite substrates correspond to the 6 mm thick panels.

5.2.3. Results from the model

The values of α and k calculated for the joints bonded with the XD4600 and SIA adhesives and loaded in modes I, II and mixed mode (I/II) are shown in Table 11. Fig. 22 shows the coefficients α as a function of k for the values given in Table 11. It can be seen that, for values of k in the range $0.3 < k < 2.25$ the greatest values of α, and hence the greatest transverse stresses, are produced by mixed-mode loading. Indeed, for the values of α and k in Table 11, the transverse stress during mode II loading was 38–45% higher than during mode I loading for the XD4600 and SIA adhesives, respectively. However, the transverse stresses induced on the loaded (upper) single substrate during mixed-mode I/II loading were 62–65% higher than during mode I loading.

Table 12 shows the calculated values of the transverse stress, σ_{yy}, induced in the composite-substrate arms during the different loading modes, using the experimental values of χ and the properties reported in Table 10 for each combination of adhesive and substrate used. Table 13 shows the same information but expressed as a percentage of the experimental transverse strength of the composite, σ_{yyc}. Values higher than 100% (shown in bold in Table 13) indicate that the transverse stresses in the substrate exceed the transverse strength. As a result, delamination would be predicted for those joints. Table 13 also shows the different failures observed experimentally, indicated in brackets in the table, for the composite substrates during mode I, mode II and the mixed-mode I/II tests. (Note that C = cohesive and D = delamination in Table 13.) It can be seen that the model shows an excellent agreement with the experimental observations for the different composite joints. When the transverse stresses exceeded the transverse strength, delamination was always observed in the experiments.

Table 10
Values of the composite transverse tensile strength and χ correction term used in the delamination model.

Composite	σ_{yyc} (MPa)		χ (−)	
	Expt.	Data sheet	XD4600	SIA
IM7/977-2	58 ± 2	73	3.3	3.1
T300/924	63 ± 1	65	2.5	2.4
HTS/6376	44 ± 5	60	2.3	2.1
Woven	20 ± 1	–	1.9	1.7

Table 11
Interaction parameter, k, and the mode dependent constants used in the delamination model.

Adhesive	k	α_I	α_{II}	$\alpha_{I/II}$
XD4600	1.44	0.29	0.40	0.47
SIA	1.62	0.29	0.42	0.48

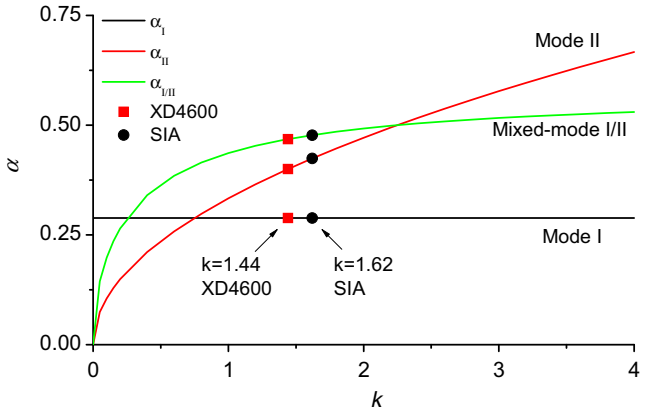

Fig. 22. Values of α as a function of the linear interaction parameter, k in the delamination model.

Fig. 23 shows the variation of σ_{yy} as a function of the G_c value for the Woven-SIA joints. The dashed horizontal line represents the measured value of the transverse tensile strength of the substrate ($\sigma_{yyc} = 20$ MPa) and the three dashed lines represent the values of G_c for cohesive failure under the different loading modes. If the vertical dashed line intersects the predicted σ_{yy} curve above the horizontal dashed line, then delamination is predicted. If the intersection is below the horizontal dashed line, then cohesive failure is predicted. Thus, this model predicts that failure in the Woven-SIA joints would be cohesive in mode I but interlaminar under mixed-mode and mode II loading. This agrees exactly with the experimental observations reported in Sections 3 and 4. At high rates, the σ_{yy} values increased somewhat for a given value of G_c as the value of k also increased with the test rate. Fig. 24 illustrates this for the T300-SIA and T300-XD4600 joints tested in mixed-mode I/II. However, the G_c values for the adhesive joints at high rates were also reduced. Hence, an overall reduction of the σ_{yy} value is expected at high rates. Delamination was predicted and observed experimentally for the T300-XD4600 during mixed-mode I/II tests at low rates. (Note however, that 10 m/s tests were not carried out for this system.)

5.2.4. Discussion of the model

The model predictions as summarised in Table 13 show that mixed-mode I/II loading induced the highest transverse stresses,

Table 12
Calculated values of the transverse tensile stress in the composite substrates, for both adhesives in the various loading modes.

Substrate	h (mm)	σ_{yy} XD4600 joints (MPa)			σ_{yy} SIA joints (MPa)		
Mode:		I	II	I/II	I	II	I/II
IM7/977-2	3	22	31	36	18	27	30
T300/924	2	45	63	74	33	49	55
HTS/6376	4	38	52	61	32	47	53
HTS/6376	6	31	43	50	26	38	44
Woven	8.5	22	30	35	19	28	31

Table 13
Calculated values of transverse tensile stress expressed as a percentage of the transverse tensile strength for the composite substrates and observed failure paths (shown in brackets).

Composite	h (mm)	σ_{yy} XD4600 joints (MPa)			σ_{yy} SIA joints (MPa)		
Mode:		I	II	I/II	I	II	I/II
IM7/977-2	3	39% [C]	54% [–]	63% [–]	31% [C]	46% [–]	52% [–]
T300/924	2	73% [C]	**101% [D]**	**119% [D]**	53% [C]	79% [C]	89% [C]
HTS/6376	4	85% [C]	**118%** [–]	**138%** [–]	72% [C]	**106%** [–]	**120%** [–]
HTS/6376	6	70% [C]	97% [C]	**113% [D]**	59% [C]	87% [C]	**100% [D]**
Woven	8.5	**108% [D]**	**149% [D]**	**175% [D]**	95% [C]	**140% [D]**	**157% [D]**

C: cohesive failure in the adhesive; D: delamination in the composite substrate; [–]: not tested.

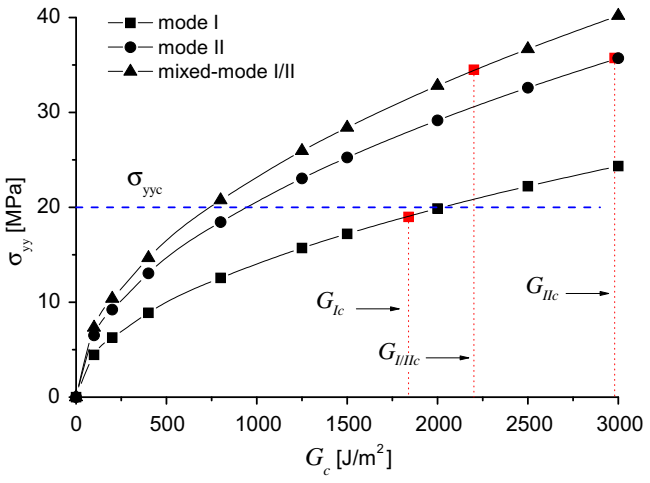

Fig. 23. Values of transverse tensile stress imposed on the composite substrate arms during the tests in each mode versus G_c for the woven-SIA joints. ($k = 1.7$).

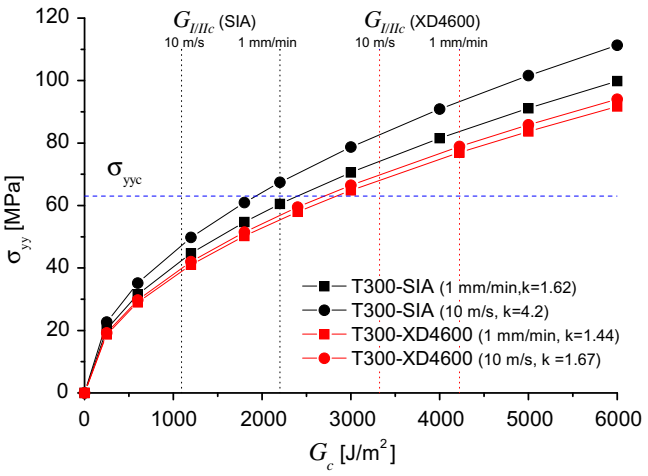

Fig. 24. Values of transverse tensile stress imposed on the composite substrate arms during the tests in the different modes versus the values of G_c for the T300-SIA and T300-XD4600 joints tested at slow and fast rates.

σ_{yy}, on the composite substrates for the different loading modes studied. This corresponds to the case when only one substrate arm was loaded, as was the case for mixed-mode. Hence, a delamination failure mode was favoured during mixed-mode loading. Furthermore, higher transverse stresses were induced when the substrates were bonded with the tougher, XD4600 adhesive than when bonded with the less tough, SIA adhesive. Hence, delamination was more likely to occur when the XD4600 adhesive was used to bond the joints.

Fig. 23 implies that the Woven-SIA joints exhibit delamination failure during mixed-mode loading when G_c exceeds a value of about 800 J/m^2 (i.e., when the mixed-mode curve intersects the horizontal dashed line). This value is in close agreement with the experimental mixed-mode value of 860 ± 220 J/m^2 reported in Table 6. However, delamination occurred at higher G_c values than predicted for the Woven-SIA joints during mode II loading. Fig. 23 predicts delamination under mode II loading when G_c exceeds a value of about 950 J/m^2. This may infer that damage in the adhesive and the composite may delay the delamination. Further, the model does not contain any information regarding the plain weave characteristics of this composite. Ultrasonic C-scans revealed some defects that had been produced during the manufacture of the 6 mm thick HTS composite panel. Although all efforts were made to avoid using material from the areas with such defects, some flaws might have remained and reduced the transverse strength of the HTS composite. This effect might have been also responsible for the higher variation in flexural strength and

transverse strength measured for this composite. Hence, lower than expected transverse properties for the HTS composite associated with high levels of transverse stress could have triggered substrate delamination. The model also shows that the value of σ_{yy} increases with increasing values of E_{xx} for the composite. This effect has also been observed in finite element simulation for similar adhesively bonded composite joints (Kinloch et al., 1992). Further, a higher substrate thickness reduces the value of σ_{yy} as shown in Table 13 for the HTS composite. Hence, for the purpose of the design of test specimens which do not display substrate delamination, an optimum composite substrate would be one from which thick panels can be produced with a relatively high transverse strength, but with low E_1 values. However, the flexural stiffness needs to be sufficient to avoid plastic deformation of the substrate arms. The composites used in this experimental work were aerospace and automotive grade composites based on tough epoxy matrices. Two solutions to avoid delamination in future tests would be the change of the composite matrix formulation to obtain better through thickness properties (e.g., using a PEEK-based matrix) and to produce thicker composite panels. However, both solutions are more expensive, difficult to manufacture and not representative of the substrates used in the automotive industry. Another possibility would be the use of other mixed-mode ratios, which could reduce the moments applied to the substrate (Charalambides et al., 1990; Blackman, 1993). Pohlit (2007) avoided delamination when testing similar Woven-SIA joints in mixed-mode I/II by using asymmetric DCB joints with G_I/G_{II} ratios of 10/1 and 2.8/1. However, this test geometry has the disadvantage that for tough adhesive systems the global mode I loading may dominate the very local mixity produced by the asymmetric substrates, producing essentially a mode I failure (Duer et al., 1995). The delamination model proposed offers a simple scheme to assess the transverse tensile stresses that can lead to delamination. The model can be further developed to include the effect of composite lay-up using analyses such as one-dimensional cylindrical bending of laminated strips (Reddy, 1997).

6. Conclusions

Adhesive joints were manufactured with composite substrates consisting of an epoxy matrix reinforced with either one of two types of unidirectional carbon-fibres or with woven carbon fibres. These substrates were bonded with one of two automotive adhesives; a single part system (XD4600) or a two part system (SIA PL731). Surface pre-treatment of the substrates always ensured that interfacial failures were avoided in the tests. Fracture mechanics tests were conducted in mode I using the DCB specimen, in mixed-mode I/II using either the FRMM or the MMF specimens, and in mode II using either the ELS or the ENF specimens. Tests were conducted in the various modes over a wide range of applied loading rates, from 1×10^{-5} m/s up to approximately 15 m/s.

High-speed video photography was used to record the specimen displacement and crack length history during the tests. Various types of crack behaviour were observed in the tests across the range of applied rates and an analysis strategy was developed to systematically analyse the fractures and determine the fracture resistance, G_c. Stable, continuous or unstable, stick-slip crack growth was observed in the joints. These were referred to as Types 1 and 4, and Types 2 and 3 respectively, depending upon whether the effects of kinetic energy were found to be significant in the tests. If the kinetic energy associated with the moving specimen arms was greater than 5% of the quasi-static value of the fracture energy of the joint then it was deemed significant and was taken into account, otherwise its contribution was neglected. Also, significant dynamic effects were always present in the tests at the faster rates which rendered the measured load values unreliable. Thus, at the faster rates the values of G_c were always deduced using a load-independent analysis.

In mode I, transitions from stable, continuous crack growth to unstable, stick-slip growth, and then back to stable, continuous growth in the adhesive layer were observed for the joints with unidirectional fibre reinforcement when bonded with the XD4600 adhesive. For this joint system, each of the Types 1–4 fracture were observed and a reduction in the cohesive value of G_{Ic} from about 3.5 kJ/m^2 to about 2.4 kJ/m^2 was measured between quasi-static and the fastest rate of 15 m/s. For the joints comprising of the woven composite substrates, then these joints failed by the fracture path running within the substrates. These delamination failures were stable, and analysis Types 1 and 4 were thus employed. The resistance to delamination failure was found to be independent of test rate. For the joints bonded with the SIA adhesive, cohesive failures were always observed regardless of whether UD or woven composite substrates were employed. However, for these joints, the quasi-static fracture behaviour was unstable, exhibiting stick-slip growth. Thus, analysis Type 1 was not invoked and Types 2–4 were used to analyse the data across the range of test rates. A reduction in the cohesive value of G_{Ic} from about 1.9 kJ/m^2 to about 0.6 kJ/m^2 was measured between quasi-static and the fastest rate of 13.5 m/s.

In mode II, two test methods were compared at slow rates, i.e., the ELS and the ENF tests were both conducted at the quasi-static rate of 1×10^{-5} m/s. For joints bonding the UD composite substrates with the XD4600 adhesive and tested using the ELS specimen, the fracture behaviour was stable, cohesive and values of G_{IIc} at both crack initiation and during steady-state propagation were deduced using a Type 1 analysis. When the woven composite was used in this joint, then the specimen exhibited delamination. When using the ENF test, then the fracture behaviour was always unstable but cohesive. Thus, only initiation values of G_{IIc} were deduced for these tests using a Type 2 analysis. For the joints bonded with the SIA adhesive, all failures were cohesive but inconsistent fracture behaviour was observed; joints using one of the UD or woven composite substrates exhibited stable failure whilst joints using the second UD substrates failed in an unstable manner. Again, the joints tested via ENF were always unstable. The analysis strategy was applied consistently; Type 1 for stable and Type 2 for unstable. Excellent agreement was always found between the values of G_{IIc} measured for crack initiation in both the ELS and the ENF tests, for either adhesive. At the faster rates, only the ENF test was used and only one UD composite substrate was studied. All failures were unstable but cohesive, and thus values of G_{IIc} were deduced using analysis Types 2 or 3. Using this analysis approach, the values of G_{IIc} were found to be quite insensitive to test rate over the range of rates studied. It was apparent however, that if the load independent analysis method was not used at the faster rates, (e.g., if Type 2 analysis was used in place of Type 3 at rates above 1 m/s) then an apparent, but erroneous, increase in G_{IIc} would have been deduced.

In mixed-mode with a loading ratio of $G_I/G_{II} = 4/3$, two test methods were compared at slow rates, i.e., the FRMM and the MMF tests were both conducted at the quasi-static rate of 1×10^{-5} m/s. The agreement between the two test methods was good for crack initiation, but the fracture behaviour observed in all joints tested in mixed-mode was dominated by delamination in the composite. At faster rates, only the MMF test was used and again only one UD composite substrate was studied. These joints also always delaminated and so no cohesive failure was recorded.

In an effort to explain the various fracture paths observed in the different tests, a model was presented in which the transverse tensile stresses exerted on the composite substrates were deduced as a function of the loading mode, the substrate properties and the cohesive toughness of the adhesive. These stresses were compared

to the measured transverse tensile strengths of the various composites to predict whether delamination would occur. The analysis showed clearly that for the adhesives studied here, the highest values of transverse stress were exerted in the tests where only one substrate was loaded, i.e., in the mixed-mode tests, and that in all modes, delamination failure was more likely to occur when the adhesive was tough, or when the substrate possessed a high value of axial modulus or a low thickness. The analysis correctly predicted that the T300-XD4600 joint would delaminate in mode II whilst the T300-SIA joint would fail cohesively and it also correctly predicted that for the woven composite substrate, only the joints bonded with the SIA adhesive and tested in mode I could fail cohesively, with all other tests using these substrates delaminating.

The analysis provides a route by which adhesively bonded test specimens can be designed to avoid the interlaminar failure mode when using composite substrates. Eqs. (17)–(19) model the relationship between the transverse stress, σ_{yy}, and the elastic properties of the substrate, the substrate thickness, and the mode I adhesive fracture energy, G_{Ic}. Thus, if G_{Ic} for the adhesive is known, and E_1 and σ_{yyc} for the composite substrate are measured, then a minimum thickness can readily be determined for the various modes to ensure that the transverse stresses on the substrate remain below the critical level required to trigger delamination during the fracture test.

Finally, the tests undertaken demonstrate that, provided failure is cohesive in the adhesive layer, values of G_{Ic} are more sensitive to increasing test rate than are values of G_{IIc}.

Acknowledgements

The authors wish to acknowledge the financial support of the EPSRC (UK), access to the EPSRC equipment loan-pool, the support of the Mexican National Council for Science and Technology (CONACYT) and the support of the Agency of Science, Technology and Research (Singapore). For material supply and collaboration we wish to thank the Predictive Technology Development and Crash Energy Management Group of the US Automotive Composites Consortium (ACC), Dr. Mike Starbuck at Oak Ridge National Laboratory, Dow Automotive, Cytec Engineered Materials and Hexcel Composites. Finally, for invaluable discussions on the delamination model, we wish to thank Professor Gordon Williams at Imperial College London.

References

ASTM (2007). Standard Test Method for the Tensile Properties of Polymer Matrix Composite Materials, ASTM International. D3039.

Blackman, B.R.K. (1993). The Fracture Behaviour of Bonded Polymeric Fibre-Composites, PhD thesis, University of London.

Blackman, B.R.K., Dear, J.P., Kinloch, A.J., MacGillivray, H., Wang, Y., Williams, J.G., Yayla, P., 1995. The Failure of Fibre-Composites and Adhesively-Bonded Fibre-Composites under High Rates of Test. Part I: Mode I Loading-Experimental Studies. J. Materials Sci. 30, 5885–5900.

Blackman, B.R.K., Dear, J.P., Kinloch, A.J., MacGillivray, H., Wang, Y., Williams, J.G., Yayla, P., 1996a. The Failure of Fibre-Composites and Adhesively Bonded Fibre-Composites under High Rates of Test. Part III: Mode II and Mixed-Mode Loading. J. Materials Sci. 31, 4467–4477.

Blackman, B.R.K., Dear, J.P., Kinloch, A.J., MagcGillivray, H., Wang, Y., Williams, J.G., Yayla, P., 1996b. The Failure of Fibre-Composites and Adhesively Bonded Fibre-Composites under High Rates of Test. Part II: Mode I Loading-Dynamic Effects. J. Materials Sci. 31, 4451–4466.

Blackman, B.R.K., Kinloch, A.J., Paraschi, M., Teo, W.S., 2003. Measuring the Mode I Adhesive Fracture Energy, G_{Ic}, of Structural Adhesive Joints: -the Results of an International Round-Robin. Int. J. Ad. & Adhes. 23, 293–305.

Blackman, B.R.K., Kinloch, A.J., Paraschi, M., 2005. The Determination of the Mode II Adhesive Fracture Energy, G_{IIc}, of Structural Adhesive Joints: An Effective Crack Length Approach. Eng. Fracture Mech. 72, 877–897.

Blackman, B.R.K., Brunner, A.J., Williams, J.G., 2006. Mode Ii Fracture Testing of Composites: A New Look at an Old Problem. Eng. Fracture Mech. 73, 2443–2455.

Blackman, B.R.K., Johnsen, B.B., Kinloch, A.J., Teo, W.S., 2008. The Effects of Pre-Bond Moisture on the Fracture Behaviour of Adhesively Bonded Composite Joints. J. Adhesion 83 (3), 256–276.

Blackman, B.R.K., Kinloch, A.J., Rodriguez-Sanchez, F.S., Teo, W.S., Williams, J.G., 2009. The Fracture Behaviour of Structural Adhesives under High Rates of Testing. Eng. Fracture Mech. 76 (18), 2868–2889.

Charalambides, P.G., Cao, H.C., Lund, J., Evans, A.G., 1990. Development of a Test Method for Measuring the Mixed Mode Fracture Resistance of Bimaterial Interfaces. Mechanics of Materials 8 (4), 269–283.

Dillard, D.A., Singh, H.K., Pohlit, D.J., Starbuck, J.M., 2009. Observations of Decreased Fracture Toughness for Mixed Mode Fracture Testing of Adhesively Bonded Joints. Journal of Adhesion Science and Technology 23 (10–11), 1515–1530.

Dillard, D.A., Pohlit, D.J., Jacob, G.C., Starbuck, J.M., Kaplan, R.K., 2011. On the Use of a Driven Wedge Test to Acquire Dynamic Fracture Energies of Bonded Beam Specimens. J. Adhesion 87, 395–423.

Duer, R., Katevatis, D., Kinloch, A.J., Williams, J.G., 1995. Comments on Mixed-Mode Fracture in Adhesive Joints. Int. Journ. of Fracture 75 (2), 157–162.

Hashemi, S., Kinloch, A.J., Williams, J.G., 1990. The Analysis of Interlaminar Fracture in Uniaxial Fibre-Polymer Composites. Proc. R. Soc. Lond. A427, 173–199.

ISO (2002). 17281 (2002)E: Plastics- Determination of the Fracture Toughness (G_{Ic} and K_{Ic}) at Moderately High Loading Rates (1m/S). Geneva, ISO.

ISO (2009). 25217. Adhesives- Determination of the Mode I Adhesive Fracture Energy G_{Ic} of Structural Adhesive Joints Using Double Cantilever Beam and Tapered Double Cantilever Beam Specimens. ISO. 25217.

Karac, A., Blackman, B.R.K., Cooper, V., Kinloch, A.J., Rodriguez-Sanchez, F.S., Teo, W.S., Ivankovic, A., 2011. Modelling the Fracture Behaviour of Adhesively-Bonded Joints as a Function of Test Rate. Eng. Fracture Mech. 78, 973–989.

Kinloch, A.J., Kodokian, G.K.A. and Watts, J.F. (1992). "The Adhesion of Thermplastic Fibre Composites". Phil. Trans. R. Soc. Lond. A.338: 83–112.

Pohlit, D.J. (2007). Dynamic Mixed-Mode Fracture of Bonded Composite Joints for Automotive Crashworthiness. Blacksburg, Virginia, USA, Virginia Tech. MS in Engineering Mechanics.

Reddy, J.N., 1997. Mechanics of Laminated Composite Plates: Theory and Analysis. CRC Press, Florida, Boca Raton.

Rodriguez-Sanchez, F.S., 2008. Fracture Behaviour of Automotive Adhesive Joints. PhD Thesis. Imperial College London.

Simon, J.C., Johnson, E., Dillard, D.A., 2005. Characterizing Dynamic Fracture Behaviour of Adhesive Joints under Quasi-Static and Impact Loading. Journal of ASTM International 2 (7), 53–71.

Starbuck, J.M., Boeman, R.G., Rastogi, N., Warren, C.D. and Carpenter, J.A. (2004). Energy Absorption in Adhesively Bonded Composites. FY 2003: Progress Report for Automotive Lightweighting Materials. Washiongton, DC, U.S. Department of Energy, Office of Freedom Car and Vehicle Technologies: 189–194.

Sun, C., Thouless, M.D., Waas, A.M., Schroeder, J., Zavattieri, P.D., 2008a. Ductile–Brittle Transitions in the Fracture of Plastically Deforming, Adhesively Bonded Structures. Part II: Numerical Studies. International Journal of Solids and Structures 45, 4725–4738.

Sun, C., Thouless, M.D., Waas, A.M., Schroeder, J., Zavattieri, P.D., 2008b. Ductile-Brittle Transitions in the Fracture of Plastically-Deforming, Adhesively-Bonded Structures: I Experimental Studies. Int. J. Solids Structures 45, 3059–3073.

Sun, C., Thouless, M.D., Waas, A.M., Schroeder, J., Zavattieri, P.D., 2009a. Rate Effects in Mode II Fracture of Plastically Deforming, Adhesively Bonded Structures. Int. Journ. of Fracture 156, 111–128.

Sun, C., Thouless, M.D., Waas, A.M., Schroeder, J.A., Zavattieri, P.D., 2009b. Rate Effects for Mixed-Mode Fracture of Plastically-Deforming, Adhesively-Bonded Structures. Int. J. Ad. & Adhes. 29 (4), 434–443.

Teo, W.S. (2008). The Performance of Adhesively Bonded Carbon Fibre Composite Joints: Pre-Bond Moisture and Rate Effects. PhD Thesis, Imperial College London.

Wall, E., Sullivan, R. and Carpenter, J. (2004). Progress Report for Automotive Lightweighting Materials. O. o. F. C. V. t. US Department of, Energy. FY2003.

Williams, J.G., 1988. On the Calculation of Energy Release Rates for Cracked Laminates. Int. Journ. of Fracture 36, 101–119.

Williams, J.G., 1989. The Fracture Mechanics of Delamination Tests. J. Strain Analysis 24 (4), 207–214.

Williams, J.G., Hadavinia, H., 2002. Analytical Solutions for Cohesive Zone Models. Journal of the Mechanics and Physics of Solids 50 (4), 809–825.